FINAL PROJECT REPORT

A Geophysical Characterization & Monitoring Strategy for Determining Hydrologic Processes in the Hyporheic Corridor at the Hanford 300-Area

PI: Lee Slater (Rutgers University-Newark, Newark, NJ, E-mail:lslater@rutgers.edu)

Co-PIs:
Fred Day Lewis and John Lane (WRD/Office of Ground Water, Branch of Geophysics, United States Geological Survey, Storrs, CT),
Roelof Versteeg (Sky Research, Hanover, NH)
Anderson Ward (Pacific Northwest National Laboratory, Richland, WA)

Other Senior Personnel:
Andrew Binley (Lancaster University, Lancaster, UK)
Timothy Johnson (Pacific Northwest National Laboratory, Richland, WA)
Dimitrios Ntarlagiannis (Rutgers University-Newark, Newark, NJ)

August 2011

Prepared for
The U.S. Department of Energy
Under Contract ER64561-1031525-0014355

Rutgers – Newark
Newark, NJ 07102

TABLE OF CONTENTS

ABSTRACT

The primary objective of this research was to advance the prediction of solute transport between the Uranium contaminated Hanford aquifer and the Columbia River at the Hanford 300 Area by improving understanding of how fluctuations in river stage, combined with subsurface heterogeneity, impart spatiotemporal complexity to solute exchange along the Columbia River corridor. Our work explored the use of continuous waterborne electrical imaging (CWEI), in conjunction with fiber-optic distributed temperature sensor (FO-DTS) and time-lapse resistivity monitoring, to improve the conceptual model for how groundwater/surface water exchange regulates uranium transport. We also investigated how resistivity and induced polarization can be used to generate spatially rich estimates of the variation in depth to the Hanford-Ringold (H-R) contact between the river and the 300 Area Integrated Field Research Challenge (IFRC) site.

Inversion of the CWEI datasets (a data rich survey containing ~60,000 measurements) provided predictions of the distributions of electrical resistivity and polarizability, from which the spatial complexity of the primary hydrogeologic units along the river corridor was reconstructed. Variation in the depth to the interface between the overlying coarse-grained, high permeability Hanford Formation and the underlying finer-grained, less permeable Ringold Formation, an important contact that limits vertical migration of contaminants, has been resolved along ~3 km of the river corridor centered on the IFRC site in the Hanford 300 Area. Spatial variability in the thickness of the Hanford Formation captured in the CWEI datasets indicates that previous studies based on borehole projections and drive-point and multi-level sampling likely overestimate the contributing area for uranium exchange within the Columbia River at the Hanford 300 Area. Resistivity and induced polarization imaging between the river and the 300 Area IFRC further imaged spatial variability in the depth to the Hanford-Ringold inland over a critical region where borehole information is absent, identifying evidence for a continuous depression in the H-R contact between the IFRC and the river corridor.

Strong natural contrasts in temperature and specific conductance of river water compared to groundwater at this site, along with periodic river stage fluctuations driven by dam operations, were exploited to yield new insights into the dynamics of groundwater-surface water interaction. Whereas FO-DTS datasets have provided meter-scale measurements of focused groundwater discharge at the riverbed along the corridor, continuous resistivity monitoring has non-invasively imaged spatiotemporal variation in the resistivity inland driven by river stage fluctuations. Time series and time-frequency analysis of FO-DTS and 3D resistivity datasets has provided insights into the role of forcing variables, primarily daily dam operations, in regulating the occurrence of focused exchange at the riverbed and its extension inland. High amplitudes in the DTS and 3D resistivity signals for long periods that dominate the stage time series identify regions along the corridor where stage-driven exchange is preferentially focused. Our work has demonstrated how time-series analysis of both time-lapse resistivity and DTS datasets, in conjunction with resistivity/IP imaging of lithology, can improve understanding of groundwater-surface water exchange along river corridors, offering unique opportunities to connect stage-driven groundwater discharge observed with DTS on the riverbed to stage-driven groundwater and solute fluctuations captured with resistivity inland.

1.0 Introduction

This final technical report describes the work conducted during the three years of funding between the dates 05/15/08-08/15/11 (report due date) at the U.S. Department of Energy (DOE) Hanford 300 Area, Richland, WA. The project tasks included (1) waterborne geophysical characterization of the Columbia River corridor (2) continuous fiber optic distributed temperature sensor (FO-DTS) monitoring of groundwater-surface water exchange, (3) land-based geophysical characterization of an area local to the Hanford 300 Integrated Field Research Challenge (IFRC) site, and (4) continuous resistivity monitoring of a zone of enhanced groundwater-surface water exchange near the IFRC identified from the DTS monitoring. These four tasks represent characterization and monitoring efforts at the 300 area over multiple scales as illustrated in Figure 1.

The broad objectives of the project were: (1) to characterize the spatial structure of the

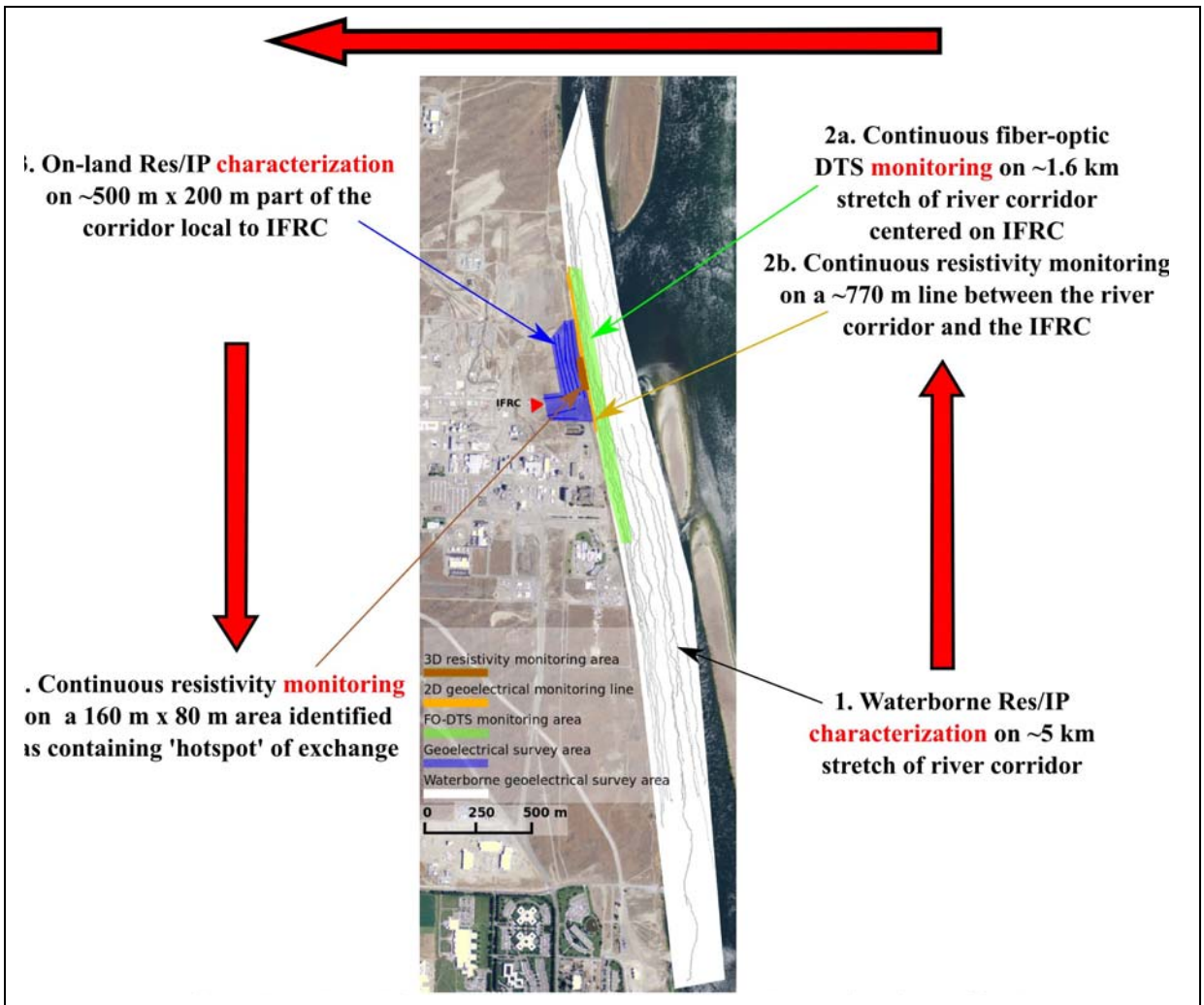

Figure 1. Summary of the multi-scale characterization and monitoring efforts performed at the Hanford 300 Area. The red triangle represents the location of the Hanford 300 Integrated Field Research Challenge (IFRC) Site

hydrogeologic framework within the near shore and sub-river bed zone at multiple scales appropriate for refining models of transport at the site; (2) to identify variability in the lateral extent of groundwater-surface water interaction; (3) to elucidate the temporal variability of groundwater-surface water interaction driven by daily and seasonal variations in stage-level; and (4) refine the high-resolution 3D stratigraphic model for part of the Hanford 300 Area by coupling geophysical data collected in the river corridor with terrestrial measurements conducted under the IFRC for this site.
The project was successful in meeting (in full or part) all the objectives identified and contributed to the development of a high resolution hydrogeological framework for the 300 Area, focusing on the local region between the IFRC and the river. In addition, the project explored novel ways to represent dynamic information on surface water-groundwater exchange captured in spatiotemporally rich temperature and resistivity datasets.

Summary of Investigator Roles and Responsibilities

This project was a strongly collaborative effort between the PI, co-PIs, other senior scientists and graduate students. PI Slater (Rutgers-Newark) was responsible for overall project management and ensuring that all tasks were completed in a timely manner. Co-PIs Lane and Day-Lewis (OGW-USGS) were responsible for the acquisition of the waterborne geophysical datasets and the installation of the FO-DTS cables along the river corridor. Co-PI Ward (PNNL) coordinated daily site activities, acquired regulatory approvals and infrastructure needed on site to support the monitoring measurements. Co-PI Versteeg was primarily responsible for the acquisition, storage and distribution of the large FO-DTS and resistivity datasets that were generated in this study.

Participant Ntarlagiannis (Rutgers-Newark) coordinated on land field data acquisition, processing and GIS database development for the project. He assisted PI Slater in all aspects of the project as needed. Participant Johnson (PNNL) was responsible for processing the 2D and 3D time-lapse resistivity datasets, whereas participant Binley (Lancaster University, UK) assisted with the inversion of the land-borne induced polarization datasets. Ph.D. student Mwakanyamale (Rutgers-Newark) played a critical role in the processing of the FO-DTS and land-borne resistivity/IP datasets and is using these datasets in her dissertation research. Ph.D. student Elwaseif assisted with the time-frequency analysis of FO-DTS and resistivity datasets.

Products and Deliverables

This work has resulted in journal articles, conference abstracts/papers and invited talks prepared by the project team. It has also provided the data for one Ph.D. dissertation project (*Kisa Mwakanyamale, Rutgers-Newark, expected completion date May 2012*). Key products are summarized below, with a full listing given in Appendix 1.

Journal Articles:

Published
Slater, L. D., D. Ntarlagiannis, F. D. Day-Lewis, K. Mwakanyamale, R. J. Versteeg, A. Ward, C. Strickland, C. D. Johnson, and J. W. Lane, Jr., 2010, Use of electrical imaging and distributed temperature sensing methods to characterize surface water–groundwater exchange regulating uranium transport at the Hanford 300 Area, Washington, **Water Resources Research.**, 46, W10533, doi:10.1029/2010WR009110[1]

In Preparation and Near Completion
Mwakanyamale, K., Slater, L., Binley, A. and D. Ntarlagiannis, Lithologic Imaging Using Induced Polarization: Lessons Learned from the Hanford 300 Area, **Geophysics**, 95% complete and submission planned for early September 2011
Johnson, T., Slater, L., Day-Lewis, F. and M. Elwaseif, Monitoring groundwater-surface water interaction using time-series analysis of resistivity datasets, **Water Resources Research**, 75% complete and submission planned for October 2011

Planned for Future Submission
PhD student Mwakanyamale will complete the processing of the FO-DTS measurements and will take the lead on two papers that will describe the time-frequency analysis of these datasets

Abstracts:
Ten conference/workshop abstracts reporting on the work have been presented, and are listed in Appendix 1

Invited Talks:
This project generated significant interest in the scientific communities engaged in studies of surface water/groundwater exchange and geophysical imaging. PI Slater gave invited keynote talks at two international workshops (NovCare, 2011 and RiskPoint 2009). Slater gave invited talks on the work at the 2009 and 2010 Fall Meetings of the American Geophysical Union. Day-Lewis gave an invited talk at the 2010 European Association of Geoscientists and Engineers (EAGE) Near Surface Meeting. Ntarlagiannis gave an invited talk at the 2010 Association of Environmental and Engineering Geologists (AEG) Annual Meeting. Other invited talks are listed in Appendix 1

[1] THIS ARTICLE WAS SELECTED AS AN AGU RESEARCH HIGHLIGHT AND A WRITE UP APPEARED ON THE BACK COVER OF THE WEEKLY AGU MAGAZINE EOS. IT WAS ALSO A HIGHLIGHTED PAPER IN WATER RESOURCES RESEARCH

Site Location: Hanford 300 Area

For over 40 years, starting in 1943, fluids containing radioisotopes and metals, generated during reactor fuel fabrication and chemical separation processes, were discharged to the shallow subsurface of the U.S. Department of Energy (DOE) Hanford 300 Area, Richland, WA (Figure 2). The primary chemical inventory included 241 metric tons of copper, 117 metric tons of fluorine, 2060 metric tons of nitrate, and between 33 and 59 metric tons of uranium (U), which is the main contaminant of concern. Previous studies have mostly focused on the behavior of U in the terrestrial system and the groundwater. A 1993 modeling study predicted that groundwater U concentrations would decrease to the 30 µg/L drinking-water standard in 3 to 10 years [*WHC*, 1993]. Based on this study, an interim decision for monitored natural attenuation with institutional controls on groundwater was implemented [*EPA*, 1996]. A review in 2006, however, showed that, despite source control measures, groundwater U concentrations remained mostly unchanged [*Hartman et al.*, 2006]. A pressing research need at this site is an improved understanding of the potential for long-term discharge of U from this persistent plume into Columbia River surface water. Achieving this understanding requires new studies that capture the spatial distribution of the primary lithologic units along the river corridor as well as spatiotemporal complexity in surface-water/groundwater exchange driven by variations in stage levels on the Columbia River. *This project was performed in an effort to obtain multi-scale information on the controls of both the underlying hydrogeologic framework and river stage on surface-water/groundwater exchange.*

Figure 2. Details and geographic location of Hanford, 300 Area site and Columbia River

Hydrogeology at the Hanford 300 site is in large part determined by two formations with distinctly different hydraulic properties (Figure 3).The uppermost unit is the Hanford Formation, containing pebble-to-boulder-size gravels and interbedded sands resulting in high hydraulic conductivity (K) of ~100 m/day [*Williams et al.*, 2007]. The underlying unit is the Ringold Formation, a highly heterogeneous unit of granule to cobble size gravels interbedded with fine sand and silt resulting in a lower K of ~0.2 m/day [*Williams et al.*, 2007]. The Hanford-Ringold (H-R) contact is generally considered an important contact that limits vertical migration of contaminants. Identifying the location of the H-R contact is likely critical to determining U distribution along the river corridor as the shape of the confining layer probably regulates contaminant discharge along the shoreline [*Fritz et al.*, 2007]. The topographic surface of the Ringold was modified by high-energy paleofloods and/or Columbia River flows that eroded into the Ringold Formation [*Brown*, 1960]. These incised channels, with a northwest-trending erosional axis, were subsequently filled with younger, more permeable Hanford Formation sediments. Although the location and distribution of paleochannels across the 300 Area is currently poorly defined, paleochannels are expected to be approximately 10-20 m in width, and they likely constrain the U plume by providing hydraulically conductive groundwater flowpaths through the region of the plume and into the Columbia River during low river stage conditions. An improved understanding of flow and transport along the river corridor of the Hanford 300 Area critically depends on mapping the locations and lateral extent of these paleochannels.

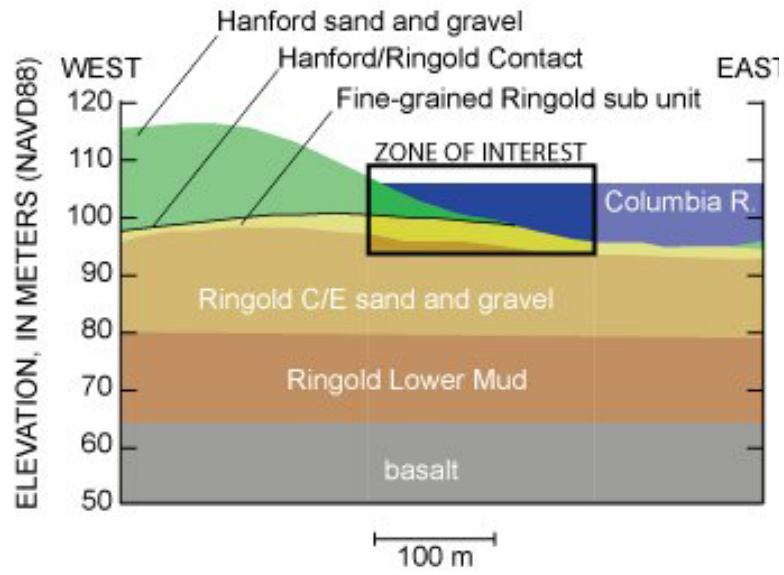

Figure 3. Generalized geologic cross-section of the 300 Area, showing the Hanford and Ringold formations, the Hanford – Ringold contact and identifying the target area of our investigation.

The current hydrogeological framework for the river corridor at the Hanford 300 Area is largely based on direct probing techniques aimed at determining the elevation of the H-R contact, and projections of the H-R contact onto the riverbed from identification in boreholes drilled inland [*Fritz et al.*, 2007]. This work supports the presence of a hydraulically resistant layer (the Ringold Formation) underlying the uppermost hydrologic unit (Hanford Formation) through

Figure 4. U concentration in the 300 Area, and estimated U contributing area [*Fritz et al., 2007*]

which surface-water/groundwater exchange and connectivity between the aquifer and surface water is most focused. Figure 4 includes an estimate of the area of the riverbed (170,000 m^2) having the potential to discharge uranium to the Columbia River, outlined in yellow and termed the estimated contributing area [*Fritz et al.*, 2007]. This outlined area represents the area that was determined to be (1) between the average river stage elevation (105 m) and the thalweg (Figure 4), (2) between the 30 µg/L concentration contours for U, and (3) sediments originating from the Hanford Formation based on determination of the top of the Ringold Formation from projections of borehole data and drive-point probes and multi-level sampling [*Williams et al.*, 2007].

Discrepancies between model predictions and field observations of U transport at the site can be attributed partly to the use of oversimplified conceptual models to describe reactive transport in a highly heterogeneous system. These models fail to consider not only subsurface heterogeneity, including the presence of possible preferential flow paths into the Columbia River and heterogeneity in and immediately beneath the stream bed, but also the effects of short term and seasonal fluctuations in river stage and the resulting interplay between surface water and groundwater. Hourly and diurnal changes in water levels in the Columbia River of over 1 m are known to give rise to some of the fastest groundwater velocities on the Hanford site and the resulting pressure wave extends as far as 1 km inland (Figure 5) [*Waichler and Yabusaki*, 2005]. These river-stage fluctuations appear to correlate with episodic changes in water chemistry, increases in groundwater U concentrations, and elevated U discharges to the river, but cannot be reproduced with the current parameterization of the Subsurface Transport over Multiple Phases (STOMP) [*White and Oorstrom*, 2006] model used

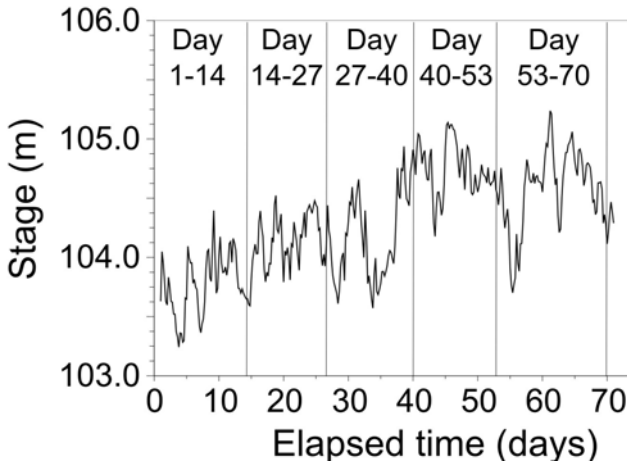

Figure 5. Example of river stage variations in the river local to the IFRC area showing non-stationary behavior

for simulation of transport at the site. Improved modeling of U transport from the aquifer into the river at the Hanford 300 site requires a more detailed characterization of lithologic heterogeneity along the river corridor, coupled with direct knowledge of spatiotemporal variability in surface-water/groundwater exchange. *Our study was designed to demonstrate how emerging hydrogeophysical technologies can address such needs at the required measurement scale.*

Overview of the main survey techniques applied in this study

A variety of waterborne and land-borne geophysical measurement methods were tested during the first field campaign in Year 1 of this project. The objective of this testing was to determine what methods provided most information with respect to satisfying the two primary project goals i.e. (1) characterizing the hydrogeological framework, and (2) determining the extent of groundwater/surface water exchange and the controls on this exchange. Waterborne test measurements included resistivity/induced polarization, seismic reflection and ground penetrating radar. Land-borne test measurements included resistivity/induced polarization, multi-frequency electromagnetics and ground penetrating radar. Ultimately, the resistivity and induced polarization technique proved most useful and was extensively utilized in this project. The second key measurement technique utilized on the river bed only was fiber optic distributed temperature sensing (FO-DTS). The fundamentals of these two techniques are summarized below.

Resistivity and induced polarization imaging

Electrical methods are based on the injection of current and mapping of the resulting electrical potentials in the earth using combinations of electrodes (Figure 6). Continuous waterborne electrical imaging (CWEI) is a recent advancement in electrical methods whereby a string of electrodes is pulled along the water surface whilst electrical measurements are continuously recorded [*Day-Lewis et al.*, 2006]. This approach results in spatially rich datasets that can be inverted for the sub-riverbed (or any water body in general) distribution of electrical conductivity ($\sigma = 1/\rho$), the reciprocal of electrical resistivity (ρ), and also the polarizability of the subsurface as explored here. In saturated sediments, such as those beneath a riverbed, the electrical

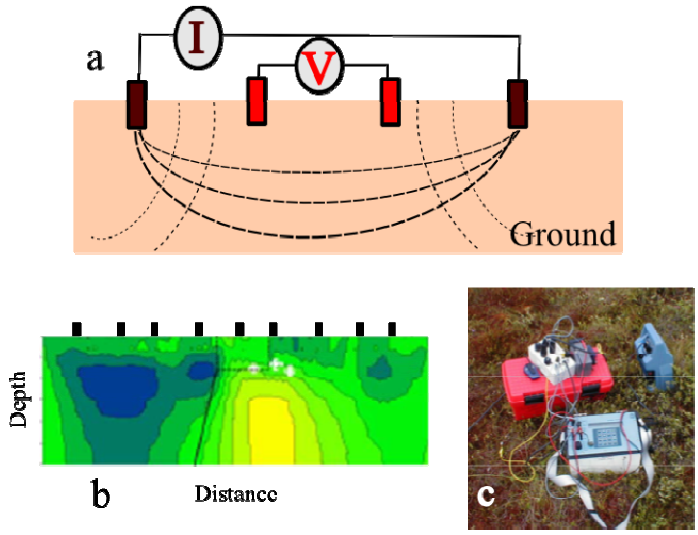

Figure 6. a) 4 electrode technique for most common resistivity / IP arrays), b) subsurface image of electrical structure is produced, c) Resistivity/IP instrument used in this study

conductivity most commonly is modeled using an empirical model with parallel electrolytic (through the interconnected pore space, σ_{el}) and surface (along the interconnected pore surface, σ_{surf}) conduction paths,

$$\sigma = \sigma_{el} + \sigma_{surf} = \sigma_w \phi^m + \sigma_{surf},$$

where σ_w is the electrical conductivity of the pore-filling fluids, ϕ is porosity and m is commonly known as the cementation factor and is determined by the connectivity of the pore space [*Archie*, 1942]. The surface conductivity (σ_{surf}) has been shown to depend linearly on specific surface area normalized to pore volume (S_{por}) of granular material both in observations [*Schon*, 1996] and theory [*Revil and Glover*, 1998]. Here, $S_{por} = S/V\phi$, where S is the sample total surface area, and V is the sample volume. Electrical methods have frequently been used to image lithologic variability in the subsurface, although the interpretation commonly is subject to considerable uncertainty due to the strong dependence of the measurements on both properties of the fluids (σ_w) as well as the sediments (σ_{surf}, m, and S_{por}). The measurements from electrical surveys are commonly reported as a transfer resistance (R), the voltage difference between two electrodes normalized by the current injected into the earth at the current electrodes. The measurements also commonly are presented as an apparent resistivity (ρ_a), calculated by multiplying R by a geometric factor determined by the relative positions of the four electrodes (units of length). The apparent resistivity is the resistivity of an equivalent homogeneous medium within the support volume of the measurement.

A valuable extension of the electrical method involves the measurement of induced polarization (IP), which records the transient voltage decay associated with temporary storage of charge in the subsurface. These measurements are often obtained concurrent with resistance measurements. At the low frequencies (<10 Hz) used in electrical surveys, electrochemical polarization is the dominant charge storage mechanism, involving a local redistribution of charge within the electrical double layer at the solid-fluid interface [*Slater and Lesmes*, 2002a]. The magnitude of this polarization is in large part determined by S_{por}, an important parameter controlling flow and reactive transport, as it represents the size of the interconnected, polarizable surface [*Slater*, 2007]. A strong linear relation between imaginary conductivity (σ''), the strength of interfacial polarization recorded with precision frequency-domain laboratory instruments, and

S_{por} recently has been shown for 114 unconsolidated soil and sandstone samples derived from seven independent datasets (see Figure 2 of *[Weller et al., 2010]*). Field IP instruments, however, usually operate in the time domain and record proxy measures of σ'' such as the normalized chargeability (M_n) parameter [*Lesmes and Frye*, 2001]. The constant of proportionality between M_n and σ'' can be determined in the laboratory, where measurements on samples are made using a frequency-domain dynamic signal analyzer that records σ'' directly, along with measurements of M_n made with the field instrument under identical configuration settings as used during the field survey.

Unlike electrical conductivity measurements, IP measurements tend to show only a weak dependence on fluid properties (e.g. σ_w), at least in soils and rocks devoid of metallic minerals [*Lesmes and Frye*, 2001]. As with electrical conductivity imaging, IP measurements are usually reported as apparent values for a homogenous earth and inverse methods are used to reconstruct the distribution of the subsurface polarizability. Inverse methods now routinely are employed to determine the best estimate of subsurface variability in conductivity that satisfies the measurement and any data (resistance and/or IP) and model constraints (e.g., [*Binley and Kemna*, 2005]). Inversions produce two- or three-dimensional cross sections or volumes of subsurface electrical properties, providing insight into spatially variable lithologic and fluid properties. Geophysical parameters commonly are functions of multiple hydrologic properties; moreover, the resolution and quality of inversions is affected by survey geometry, measurement error, and inversion settings [*Day-Lewis et al.*, 2005]. For these reasons, it is critical to interpret geophysical results jointly with other data types, such as direct hydrologic measurements and temperature data.

Fiber-optic distributed temperature sensing (FO-DTS)

Fiber-optic distributed temperature sensing (FO-DTS) is an emerging technology with applications in fire detection, industrial process monitoring, and petroleum reservoir monitoring, with more recent implementation to obtain spatially rich datasets for monitoring surface-water/groundwater exchange in streams, lakes, marshes, and estuaries (e.g., [*Henderson et al.*, 2009; *Moffett et al.*, 2008; *Selker et al.*, 2006a; *Selker et al.*, 2006b; *Tyler et al.*, 2009]). The sensor consists of standard telecommunications fiber- optic cable (Figure 7). FO-DTS measurement physics is based on temperature-dependent backscatter mechanisms including Brillouin and Raman backscatter [*Selker et al.*, 2006a] (Figure 7). Most commercially available systems, including the unit used here, are based on analysis of Raman scatter. As laser light is transmitted down the fiber-optic cable, light scatters continuously back toward the instrument from all along the fiber, with some of the scattered light at frequencies above and below the frequency of incident light, i.e., anti-Stokes and Stokes-Raman backscatter, respectively. The ratio of anti-Stokes to Stokes energy provides the basis for FO-DTS measurements. Measurements are localized to a section of cable according to a time-of-flight calculation (i.e., optical time-domain reflectometry). Assuming the speed of light within the fiber is constant, scatter collected over a specific time window corresponds to a specific spatial interval of the

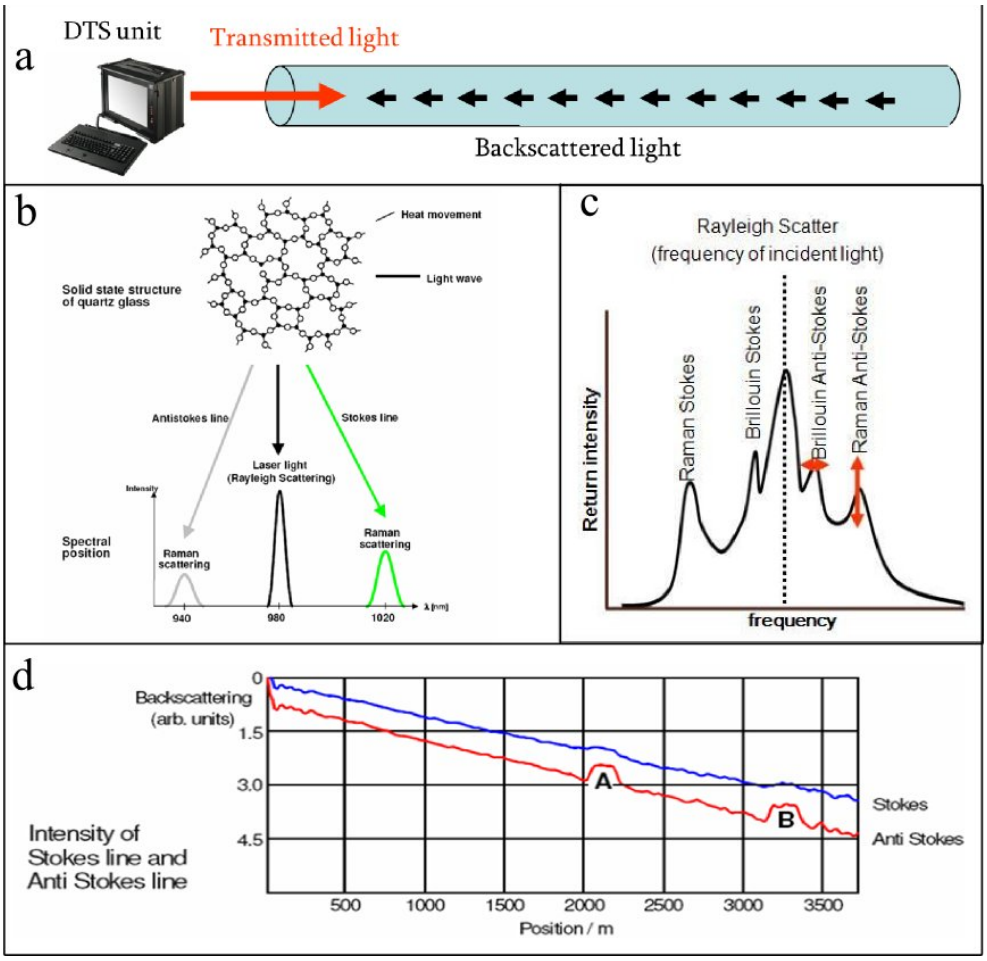

Figure 7. Summary of the FO-DTS measurement technique (a) method overview depicting FO-DTS cable connected to source/receiver, (b) scattering mechanisms originating on quartz glass, (c) Rayleigh scatter showing Raman components used in FO-DTS measurements, (d) Stokes and Anti-Stokes scattering components used to estimate temperature

fiber. Although there are tradeoffs between spatial resolution, thermal precision, and sampling time, in practice it is possible to achieve meter-scale spatial and 0.1°C thermal precision for measurement cycle times on the order of minutes and cables extending several kilometers [*Tyler et al.*, 2009]; thus, thousands of temperature measurements can be made simultaneously along a single cable. This emerging technology is ideal for generating spatially rich thermal maps that can visualize a large amount of temperature data and quickly identify major trends in surface-water/groundwater exchange.

2. Regulatory issues addressed to permit measurements on the river corridor

Various site access and regulatory approvals were required for conducting research at the site and ensuring that the various types of infrastructure needed to support long-term FO-DTS and resistivity monitoring were in place. A health and safety plan was first developed for the site to govern general field activities such that all work performed by the various independent

collaborators (Rutgers University, the United States Geological Survey, and the Idaho National Laboratory) under the coordination of the Pacific Northwest National Laboratories (PNNL), would be performed in a safe and conscientious manner.

Cultural and Ecological Resources Review of the Field Site

Prior to the installation of any field instrumentation or the collection of any data on the river or riverbed, it was necessary to conduct a cultural and ecological resources review of the site. Per 36 CFR 800, on January 18, 2008, the Washington State Historic Preservation Office (SHPO), Yakama Nation, Nez Perce Tribe, Wanapum, Confederated Tribes of the Umatilla Indian Reservation, and the Confederated Tribes of the Colville Reservation were notified of the Area of Potential Effect (APE) related to the project. The APE was defined as being confined to the project areas delineated in Figure 8. SHPO concurred with this APE on January 22, 2008. The project scope was initially presented at the DOE-RL Cultural and Historic Resources Program (CHRP) tribal cultural resources at an earlier meeting in October 23, 2007.

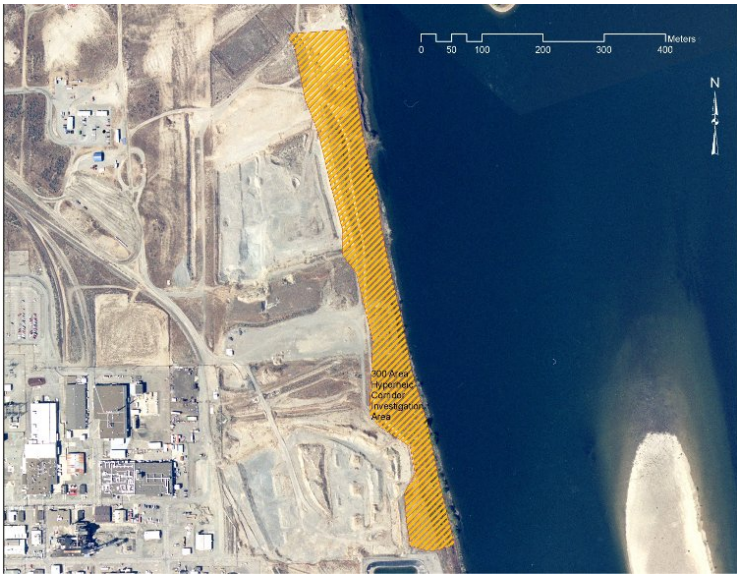

Figure 8: Area of Potential Effect (APE) archaeological site boundary overlaid on a 2006 aerial photograph of the river corridor at the Hanford 300 site

A records and literature search was conducted to identify previous cultural resources investigations and cultural resources located within the vicinity of the survey area. This search revealed the APE has been investigated numerous times for various projects since 1948. Within the initial confines of the field-site boundary, some 50 pre contact-era sites have been identified and are listed in the Washington State Heritage Register in 1983. Present at these sites was significant archaeological material with relative dates ranging from 7000 years before present to the early twentieth century. Based on multiple documented dates associated with sites and the presence of intact buried archaeological deposits, observed in past archaeological excavations and observable in the cut bank in 2008, it was recommended that the site be eligible for the National Register of Historic Places because the property yielded, and is likely to yield, information important in prehistory. Tribes expressed concern about the appropriateness of collecting geophysical data over areas that contain human remains and that may not be appropriate for this area. Following the Section 106 review process, it was recommended that the site boundaries be moved to the south to avoid a site with human remains.

It was concluded that the field study should not adversely affect historic properties provided scientists and field technicians were made aware that they are in an archaeological site and are instructed not to pick up artifacts. No more than three technicians should be present within the archaeological site boundary at one time to minimize foot traffic through the site. Intermittent cultural resources monitoring by a professional archaeologist was deemed necessary.

Approvals for Work on the Columbia River

Activities in or near the Columbia River have the potential to kill fish or shellfish directly. More importantly, these activities can potentially alter the habitat that fish and shellfish require, which could lead to direct loss of fish and shellfish production. As a result, installation of the fiber optic distributed temperature sensors (DTS) cabling and the performance of the waterborne geophysical surveys required a hydraulic project approval, from the Washington State Department of Fish and Wildlife (WDFW). A review of the submitted documents and a telephone interview by the Area Habitat Biologist for Yakima, Franklin, and Benton counties concluded that the installation of the FO-DTS cables as described was non-invasive and would not require a hydraulic project permit.

Figure 9. GPS determined tracks of the CWEI surveys

3. Methods

a. Continuous Waterborne surveys (CWS)

The coverage of the waterborne surveys is shown in Figure 9. Water depths varied substantially across the surveyed area from a minimum of 2 m close to shore to a maximum of 18 m when crossing the channel thalweg (Figure 10). The surveyed area is approximately centered on the Hanford 300 Integrated Field Research Challenge (IFRC). The waterborne surveys included resistivity/induced polarization (R-IP), ground penetrating radar (GPR) and seismic reflection. Preliminary surveys showed that the resistivity/IP measurements were the most effective technique for mapping the Hanford-Ringold contact. The GPR and seismic measurements were of very limited value as both methods were adversely affected by the site conditions, primarily the cobble framework of the bed. Approximately 30 km of R-IP data were collected relative to only 9 km of GPR and seismic data. The datasets were acquired during a field

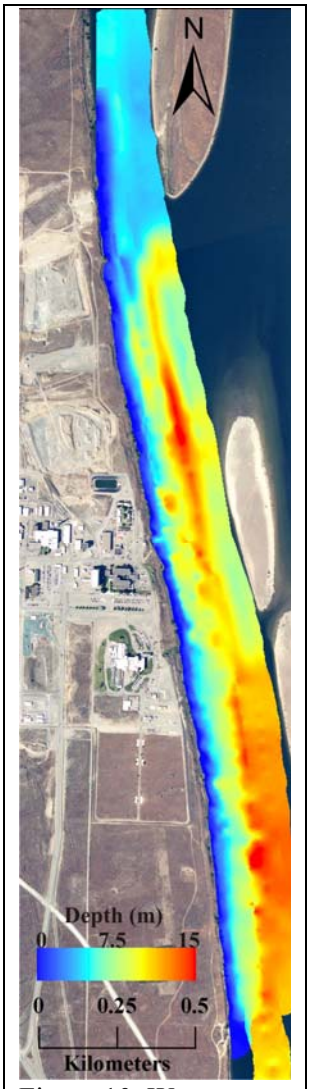

Figure 10. Water depths recorded during the CWEI survey.

campaign in July 2008, as relatively high water levels facilitated surveying close to the western bank of the river. All datasets were acquired from a *Gregor* 21-ft aluminum hull jet boat (Figure 11), equipped with a 105 hp outboard motor, owned by the USGS operating out of its Seattle office. Water depth was continuously measured using a *Garmin GPSmap 420s* equipped 200/50 Khz – 10/40 degree depth finder transducer (estimated accuracy of 50 cm based on field tests) during all surveys (Figure 10). All measurements were geo-referenced using a GPS (*Garmin GPSmap 420s*) unit with ± 0.5 m accuracy.

Continuous waterborne electrical imaging (CWEI)

CWEI surveys were conducted using a 10-channel time-domain resistivity/IP instrument (Syscal Pro, Iris Instruments, France). This time-domain instrument records the polarizability as an apparent integral chargeability (*Ma*) determined from the decay curve after current shutoff. All data were acquired using a 13-electrode cable with graphite electrodes spaced at 5 m intervals. The configuration of the 10 measurement channels was chosen so as to (1) provide a high signal-to-noise ratio for all 10 channels (critical to collecting reliable IP data), (2) result in a desirable sensitivity pattern relative to other common configurations [*Mansoor and Slater*, 2007], and (3) optimize the 10-channel capabilities of the instrument. Measurements were recorded every 0.5-3.0 m depending on survey speed (in part dictated by strong currents on the Columbia River), resulting in ~65,000 measurements conducted on ~30 km of line.

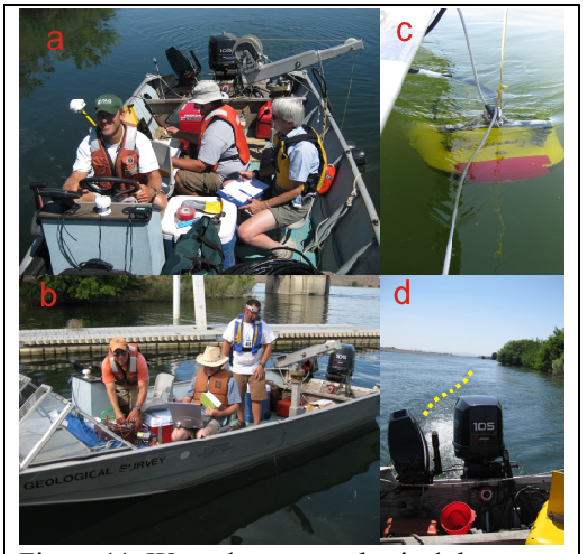

Figure 11. Water-borne geophysical data collection: a) GPR – seismic, and b) ρ / IP field crews; (c) chirp seismic unit, d) ρ / IP survey showing towable graphite electrode string (yellow dots superimposed on electrodes for clarity).

CWEI surveys (i.e. with the boat and cable in motion) do not permit application of standard methods for assessing measurement error (e.g., repeatability/stacking tests and/or reciprocity). However, surface electrical measurements are inherently low resolution and it is therefore reasonable to expect a smooth distribution of apparent resistivity and apparent chargeability

over most natural geologic structures. Furthermore, it is justifiable to remove values inconsistent with the physics of electrical current flow. For example, although it is possible to record negative apparent chargeability in the presence of strong geometrical effects, such effects were not expected here. In the resistivity dataset obvious outliers are those measurements with a very small resistivity close to 0 Ohm m, a physically unreasonable result given the soils at this site. These considerations resulted in ~2% of the dataset being removed from the inversion. Confidence in the mapped variability of ρ_a and *Ma* along a two-dimensional (2D) line was also established by comparison with ρ_a and *Ma* structure observed on adjacent parallel lines (Figure 12). Data quality was very good with only 1.2 percent of the data points removed as likely outliers before further processing. Figure 12 is an example of the distribution of ρ_a and *Ma*, with the data showing strong variability both perpendicular (E-W) and parallel (N-S) to the river bank. These plan views of the shore-perpendicular variability in part reflect the substantial increase in water depth towards the channel center. However, it is the shore-parallel variability that is of most interest here as we wish to determine variability of the hydrogeologic framework along the river corridor at the Hanford 300 Area.

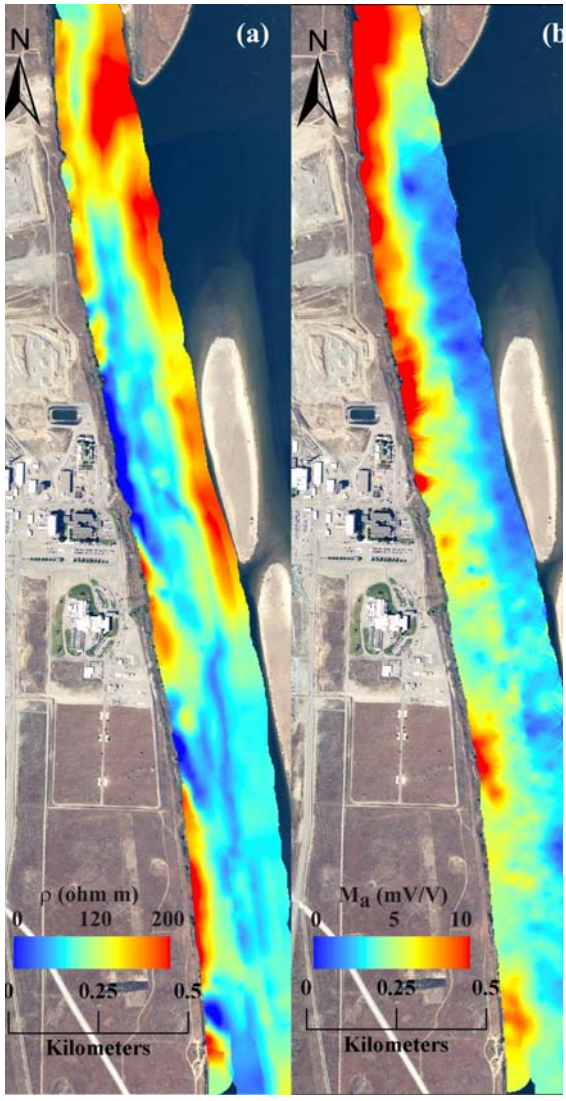

Figure 12. a) apparent resistivity (ρ), and b) apparent chargeability (m) distribution for the CWEI surveyed area

The CWEI dataset was inverted for an estimated subsurface distribution of resistivity and chargeability using the RES2DINV package [*Loke et al.*, 2003] as it efficiently handles large datasets and permits a variable thickness water layer of uniform resistivity and zero chargeability (water is non-polarizable at low frequencies) to be incorporated as an inversion constraint. A uniform resistivity water layer is a valid assumption considering the fact that the survey was run during very high stage conditions when we will show that focused groundwater discharge is suppressed such that the physical properties of the water column are likely to be relatively uniform. Measurements made with the shortest electrode separations, almost exclusively sensing the resistivity of the water column, support this assumption. For example, along Line 20 m the mean apparent resistivity of the shortest electrode spacing was 99 Ohm m with a standard deviation of 17 Ohm

m. Given the significant discrepancy between the sample density shore-parallel (1 measurement every few meters) and shore-perpendicular (1 measurement every ~20 m), the dataset was treated as a series of near-parallel 2D lines. True electrode locations (calculated from the boat location and the azimuth of the electrode cable behind the boat) were first projected onto a best-fit 2D line. Each line was then inverted for a 2D electrical structure along the river corridor using the common smooth regularization constraint (whereby model structure is minimized subject to fitting the data to some acceptable tolerance) [*de Groot-Hedlin and Constable*, 1990]. These 2D inversion results were then interpolated in ArcView to generate a pseudo three-dimensional (3D) dataset of ρ and M variation within the surveyed volume of the river corridor.

Waterborne GPR and seismics

The quality of waterborne chirp seismic and GPR methods depends on whether or not the streambed is armored, how deeply electromagnetic and sound waves penetrate, and the presence of gases. The widespread presence of cobbles on the Columbia River was expected to limit application of these techniques. However, the modest additional cost of GPR and seismic collection was considered to make these surveys worthwhile given availability of the personnel, boat and auxiliary equipment (depth finder, GPS) necessary for resistivity-IP work. Approximately 6 km line of boat-towed ground penetrating radar (GPR) data was collected with a 100-MHz Mala shielded antenna. Approximately 10 line-km of boat-towed chirp-seismic data was collected using an EdgeTech SB-216 and SB-424 instrument. Inspection of the data indicates that GPR data provides some information about bed material (fine-grained Ringold vs. coarse-grained Hanford formations), but little signal is returned from below the streambed, except in a few isolated regions where some stratigraphy is recovered. Inspection of the seismic data indicated that the bed reflection is strong over most of the survey area, but lacking in deeper reflection returns, thereby preventing interpretation of sub-bottom structure. As we shall show, the resistivity/IP datasets proved very successful in achieving the objective of mapping the major hydrogeological framework along the river corridor, so further processing of the GPR and seismic datasets was considered unnecessary. Representative datasets from the waterborne seismic and GPR surveys are presented in Figures A1 and A2 of Appendix 2.

Ground penetrating radar measurements were also collected along lines on the river bed but against the channel edge, where a watercraft was not required. The length of the river corridor depicted by the western most line of the CWEI survey shown in Figure 9 was covered with this survey. As with the waterborne GPR survey, most of the data recorded on these lines did not provide useful information due to the combination of limited penetration and scattering of energy from the cobbles making up the river bed. One notable exception was observed towards the north of the investigation area where this survey identified evidence for a depression in the Hanford-Ringold contact with characteristics expected of a paleochannel (Figure 13). In fact, the feature recorded shows many similarities with paleochannel features observed in vintage GPR datasets acquired inland ([*Kunk and Narbutovskih*, 1993]) (Figure 13). This dataset provides evidence of paleochannels connecting with the Columbia River. The location coincides with a temperature

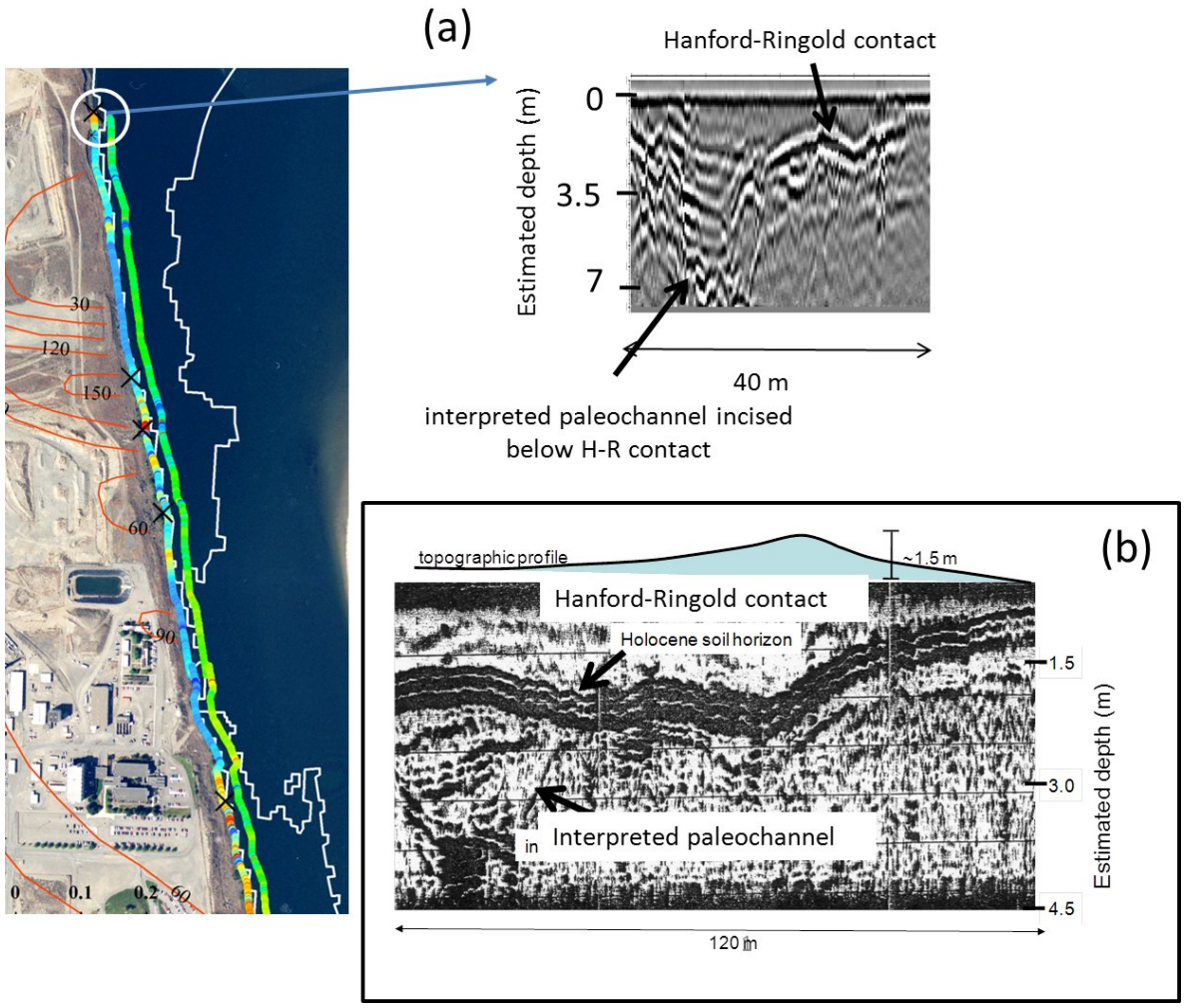

Figure 13. (a) GPR evidence for a paleochannel at the north end of the river corridor investigated in this study, coinciding with a temperature anomaly and a know uranium seep (Fritz et al., 2007). (b) example of paleochannel features mapped in vintage GPR datasets inland and west of the IFRC (Kunk et al., 1993)

anomaly depicted in the FO-DTS dataset. As discussed below, these anomalies are indicative of focused groundwater-surface water exchange. No similar features were identified at other locations along the line, including around the IFRC site, being the focus of this study (Figure 1).

b. Fiber Optic Distributed Temperature Sensing (FO-DTS)

In November 2008 four armored fiber-optic measurement cables were installed semi-permanently on the bed of the Columbia River centered on the Hanford 300 Area (Figures 14, 15) Although a zigzag or grid pattern would be an optimal deployment and several bank-perpendicular transects would provide additional information, cables oriented cross-flow would more likely snag floating debris and would be subjected to the full force of the current. Given the high currents associated with this river, we opted for a series of four parallel cables at different distances between 2 m and 20 m from the riverbank (Figure 15). These cables were continuously

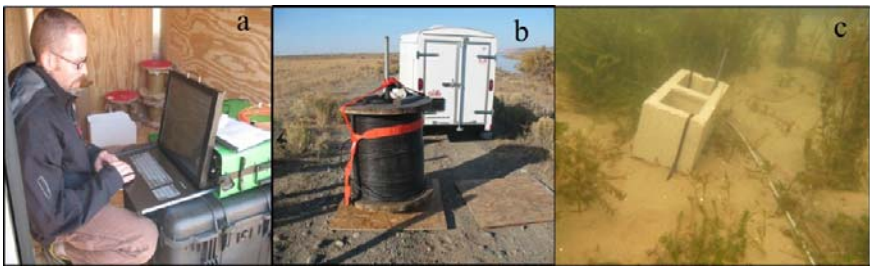

Figure 14. a) Control unit and PC for the FO-DTS system; FO cable b) before, and c) after installation where heavy weights used to anchor the cable

below the water surface (even at the lowest stage during the data acquisition) throughout the length of the study reach. In this report, we focus on analysis of data from a ruggedized, ~ 1-cm diameter,1.6-km long Sensornet EnviroFlex cable that was deployed 2 m from the bank by a team operating on foot in waders, with the cable manually secured to the stream bed using stakes, cinder blocks, and native cobbles. GPS data were recorded at discrete locations along the cable (Figure 15). The FO-DTS unit was programmed to collect data every meter along the cable at a 5-min time interval. A Sensortran 8-channel Gemini control unit was set up and calibrated using ice-and-water baths as well as the stream and air temperatures (Figure 14). The system was remotely accessed with data routinely transferred to a remote server (Figure 14).

c. Land borne surveys.

Topography onshore close to the Hanford 300 IFRC presents challenges for land-borne data acquisition proximal to the river (Figure 16). Trials were performed with resistivity/induced polarization, GPR and multi-frequency Slingram electromagnetic induction (EM) measurements. A ~750 m resistivity/IP survey was performed as close as possible to the channel edge (Figure 17). GPR tests were conducted on 45 m profiles using a Mala unshielded system and a range of antenna frequencies (25, 50, 100 and 200 MHz) (Figure 17). In all cases GPR signal penetration was limited presumably due to high attenuation coefficients associated with the relatively fine shore bank soils. These findings are consistent with surface GPR measurements made on the 300 Area IFRC site [*Ward and Clemment*, 2005]. These on land GPR surveys therefore provided limited useful subsurface information and were subsequently not collected along the entire line length. The EM measurements were performed with a multi-stepped frequency GEM-2 (Geophex Inc.)

Figure 15. Location of the four FO-DTS cables compared to the IFRC

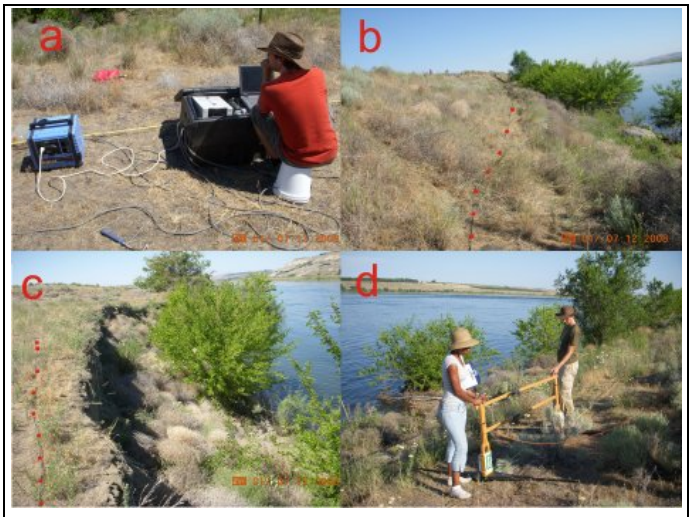

Figure 16. a) Resistivity / IP control unit, b – c) resistivity – IP line on the ground (red dots superimposed for better visualization) d). GPR data acquisition

instrument. Trials on ~1 km of line showed that, although the instrument was very sensitive to buried metallic objects, the site was generally too electrically resistive to permit effective mapping of the hydrogeologic framework.

These trial measurements conclusively demonstrated that resistivity and induced polarization measurements offered the best approach to determining information on the hydrogeologic framework and groundwater/surface-water exchange inland from the river corridor. Three land-borne electrical geophysical surveys were therefore conducted to address different scales during this project (Figure 1). Firstly, an induced polarization survey was conducted primarily over a ~500 m x 200 m area in an effort to map variations in the depth to the Hanford-Ringold contact between the IFRC and the river corridor. Secondly, two resistivity monitoring surveys were performed in an attempt to monitor groundwater-surface water interaction inland away from the river bed.

Figure 17. Location of the trial GPR, EM and Resistivity – IP land borne surveys

Land borne induced polarization imaging of the hydrogeological framework

These surveys were performed in an effort to map variations in the depth to the Hanford-Ringold contact between the IFRC and the river corridor. A particular focus was the identification of possible depressions in the elevation of the H-R contact, e.g. due to paleochannels, that might act as preferential flow and transport paths that could locally enhance exchange. Two-dimensional (2D) time domain resistivity/IP surveys were carried out in the 300 Area between IFRC and the river corridor (Figure 1). Figure 18 shows the location of ten resistivity/IP profiles covering about ~3 km of line length. Seven profiles running approximately parallel to the river were spaced ~20 m apart, Line 0 being nearest (about 10 m from) the river. Line 0 was purposely close to the river in an effort to locate evidence of any paleochannels in direct contact with the

riverbed. Three additional profiles were run orthogonal to the river towards the IFRC area. The lack of borehole datasets for ground-truth in our survey area represented a confirmation challenge at the beginning of our investigation. However, the recently drilled boreholes, 399-1-57 (C7656) and 399-02-01, within our survey area (Figure 18) provides indispensable information that we later use to ground truth our geoelectrical survey results.
An additional 2D IP line was performed to the north of the IFRC site. This location was investigated due to anomalies in the CWEI survey, the initial FO-DTS and land GPR surveys (Figure 13). This location was as close as possible to a sandy area on the river bed that showed IP and temperature anomalies as well as a prominent event in the ground penetrating radar (GPR) reflection record with characteristics of a paleochannel (Figure 13).

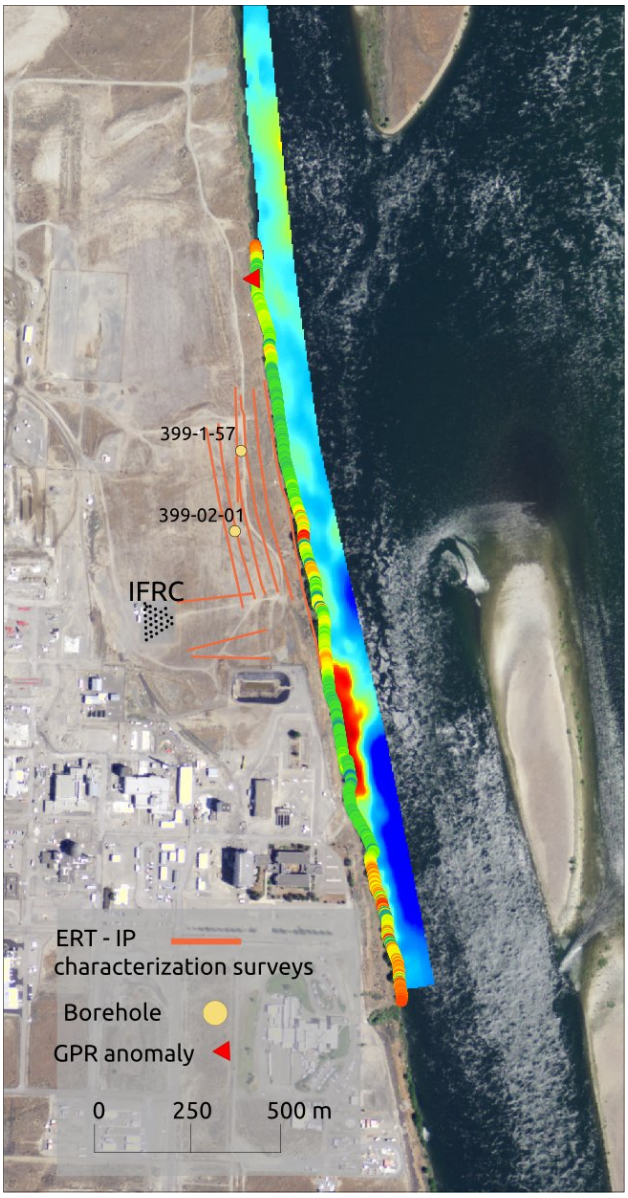

Figure 18. Profiles of time domain resistivity/IP imaging survey lines adjacent to the Columbia River in Hanford 300 Area, Richland, Washington centered on T and Mn anomalies. Yellow dots indicate wells that we used to confirm H/R contact depth.

All datasets were acquired with a 10-channel Syscal Pro (Iris Instruments, France) time domain resistivity/IP meter. For IP data acquisition, a total of 20 windows were sampled using a current waveform with a 1s on time, 1s off time, a 0.12 s delay time and total window length of 20 s. Stainless steel electrodes were used in the field with various spacing depending on the number of electrodes in the cable used and location of the survey profile. The data acquisition sequence used a combination of array types, including short offset dipole-dipole, nested dipole, Wenner, and skip two dipole types. These configurations were selected as they provided a good compromise between signal strength and resolution. A complete set of reciprocal resistivity and IP measurements was acquired to facilitate error assessment.

Resistivity monitoring of groundwater/surface water exchange inland from the river

The first resistivity monitoring survey was performed on a 2D profile spanning 755 m of the river corridor under investigation. The scale of this survey was selected to be similar to that of the FO-DTS survey in order to investigate how multiple points of focused exchange located in FO-DTS datasets would be expressed by mixing inland. The second monitoring survey was a higher resolution, pseudo-3D survey focused at a point of high interest close to the IFRC where FO-DTS anomalies indicate focused exchange, and induced polarization surveys (and available borehole data) support the presence of a depression in the H-R contact that could channelize exchange between the IFRC and the river.

Resistivity monitoring along the river corridor

During a spring 2009 field campaign we installed a 2D ERT monitoring system for investigating surface water-groundwater exchange (Figures 19). The system consisted of 155 electrodes, at 5m spacing, spanning over ~770 m of the river corridor, close to the Hanford IFC. This continuous resistivity monitoring system was controlled by a single channel MPT technologies resistivity and IP system. The control unit, transmitter, and monitoring pc were housed in a trailer with temperature control (A/C during summer, heating during winter) to ensure proper operation. Due to the length of the monitoring area two satellite muxes (multiple connectors to electrodes) were installed 150 m north and south of the trailer, located in the midpoint of the survey line; these satellite muxes were housed in ruggedized field boxes and the power and signal lines were protected (e.g. from animals) by pvc conduit. Due to the site conditions (mainly very high contact resistances during summer months) the system required an additional dedicated summer field campaign to test and calibrate the set up. Following optimization, the system started data acquisition in September of 2009. The optimized measuring sequence consisted of ~6500 measurements with reciprocal measurements recorded for error assessment. The system was set to run continuously, and collect 4-5 frames of data per day. The set up was wirelessly connected to the internet and data acquisition and system performance were diagnosed on-line via a desktop sharing platform. Due to weather and hardware problems the system was collecting data intermittently for almost a year. We were ultimately successful in collecting continuous data from May to July 2010.

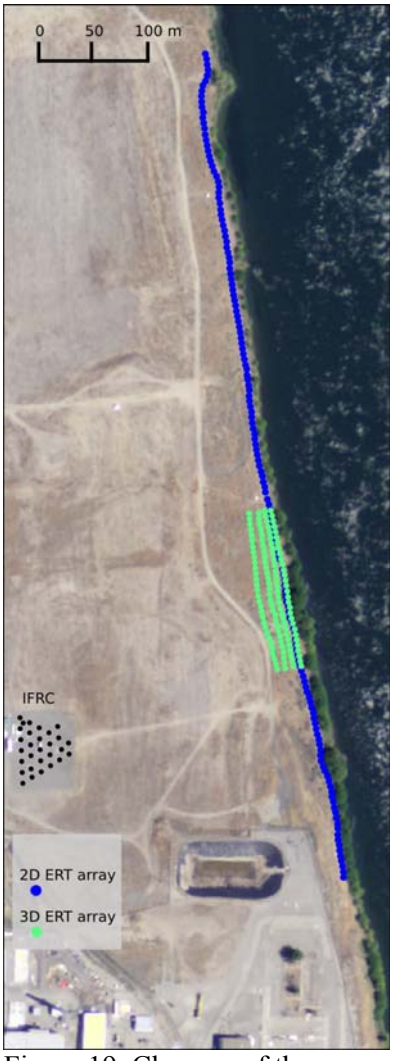

Figure 19. Close up of the location of the 2D and 3D ERT monitoring arrays

Focused 3D monitoring close to the IFRC

In October of 2010 we installed a 3D resistivity array immediately east of the IFRC and close to the river (Figures 19-20). The 3D array was centered on a section of the river corridor slightly north of the IFRC, where results of CWEI and FO-DTS analysis identified thick Hanford sediments coincidental with a large number of temperature anomalies indicative of focused groundwater/surface water exchange (Figure 20). Resistivity data were acquired using ERTLab 8, a multi-channel resistivity monitoring system produced by MPT technologies (NV). The 3D array was constructed using 120 copper electrodes placed at 5 m spacing along each line. Four lines were oriented parallel to the river bank and spaced approximately ~ 5 m apart, with minor variations depending on the relief and vegetation. All four parallel lines contained 30 electrodes. All electrode locations were geo-referenced using a high precision RTK-GPS system, providing sub-centimeter precision when referenced to a benchmark on site. Data were acquired using a combination of dipole–dipole and gradient electrode geometries. These geometries were selected based on trial measurements that considered signal to noise ratio at the site, as well as acquisition rates. A complete set of reciprocal measurements, whereby the voltage and current electrode pairs are exchanged, was obtained for calculation of individual data errors used in the inversion. The total dataset consisted of 19,354 measurements (including reciprocals) and took 2.5 hours to collect. The monitoring system was operated continuously and resulted in a large number of datasets, and mandating the use of time series analysis and time-frequency analysis to concisely represent the information on exchange captured in this dataset. In total, 273 data sets were collected from Nov. 17, 2010 to Feb. 22, 2011 to produce bulk conductivity time series that are compared to river stage in the forthcoming sections.

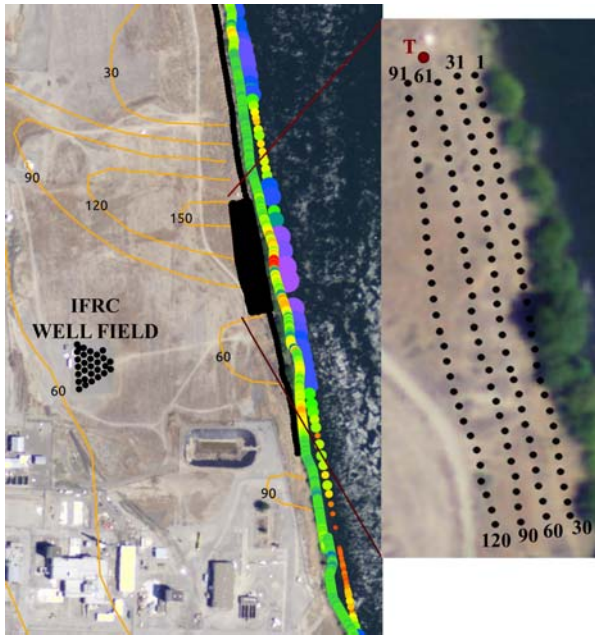

Figure 20. Location of the 3D monitoring ERT array relative to the IFRC, T anomalies and estimated H-R contact depth. The location of a string of T sensors is also shown

Time-series analysis of FO-DTS and 3D resistivity datasets

The FO-DTS and 3D resistivity time-series datasets provided records of temperature or resistivity with high spatiotemporal resolution. In our studies temperature was recorded at 5 min intervals with a spatial resolution of 1-2 m along the cables. The temporal resolution of the 3D resistivity imaging was much lower (~4 datasets/day) but the spatial information is rich in this

dataset. Statistical descriptors of the relationship between the stage and temperature/resistivity datasets were employed to better understand the control of stage on these geophysical measurements.

Two properties were assessed and described below. For simplicity, the equations are just written for the example of bulk conductivity obtained from the 3D resistivity survey, but the same equations can be written for temperature determined from FO-DTS.

Correlation: The correlation between bulk conductivity and stage at time lag *t* is given by

$$corr(t) = \frac{1}{N_t}\sum_{k=0}^{N_t-t}\left(\frac{C_k-\bar{C}}{\sigma_C}\right)\left(\frac{S_{t+k}-\bar{S}}{\sigma_S}\right) \quad (1)$$

where N_t is the number of stage and conductivity values in the time sequence, C_k is the bulk conductivity at time *k,* $\bar{C}$ is the mean conductivity of the time sequence, σ_C is the standard deviation of the conductivity time sequence, S_k, $\bar{S}$ and σ_S are the corresponding stage time series, mean, and standard deviation. In terms of temperature, the sign of the correlation is expected to vary with season. A negative correlation is expected in the winter as falling stage will result in discharge of warmer groundwater, with a positive correlation expected in the summer when falling stage will result in discharge of cooler groundwater. In the case of resistivity, a negative correlation between river stage and bulk conductivity is expected assuming that higher stage levels drive less conductive river water into the aquifer.

Lag time to maximum correlation: The time lag t_{max} to maximum absolute correlation represents the time required for the stage to reach either the point on the FO-DTS cable or the voxel in the 3D resistivity survey. Considering the 3D resistivity survey, elements further from the river should exhibit longer time lags to maximum correlation than elements next to the river. Furthermore, elements in more permeable zones connected to the river should exhibit shorter lag times because pore water will travel more quickly in these zones give the same stage induced gradient. Lag time to maximum correlation was therefore expected to be indicative of preferred flow channels.

We also recognized an opportunity to further improve our interpretation of these datasets using time-frequency analysis. Indeed, studying the frequency content of geophysical time series has proven an effective approach for enhancing the information extracted from the datasets (e.g., [*de Voogd*, 1983; *Sinha et al.*, 2009]). The Fast Fourier Transform (FFT) has been applied widely to process different geophysical data (e.g., [*de Voogd*, 1983; *Denker and Wenzel*, 1987]). However, the FFT method is unsuitable for analyzing non-stationary geophysical time series such as the FO-DTS and 3D resistivity systems have recorded since the method only provides time-averaged amplitude and it does not provide information about the changes of frequency content with time (e.g., [*Stockwell et al.*, 1996; *Tsoulis*, 2003]). To address the FFT limitations, the Continuous Wavelet Transform (CWT) has been applied extensively to analyze nonstationary signals (e.g., [*Gamage and Blumen*, 1993; *Grinsted et al.*, 2004; *Haus and Graber*, 2000]). The drawback of this method is that it attenuates high frequency signals [*Liu et al.*, 2007].

In this work we made use of an S-Transform to examine the time dependent frequency content of the FO-DTS, 3D resistivity and associated river stage datasets. Unlike the FFT and CWT, the S-Transform combines a frequency-dependent resolution of the time-frequency space with absolutely referenced local phase information [*Stockwell*, 1999]. Stockwell (1999) derives the S-Transform from the Short Time Fourier Transform (STFT) as follows; the time average spectrum *H(f)* for a given time series *h(t)* is given by

$$H(f) = \int_{-\infty}^{\infty} h(t)g(t)e^{-i2\pi ft}dt, \ldots\ldots\ldots (2)$$

where, *f* is the frequency of different periods within the signal, *t* is time and *g(t)* is a Gaussian function used to window the time series *h(t)*.

The S-Transform uses a Gaussian function with a width depending on the local frequency under investigation, the dilation (τ) and translation of the wavelet. The Gaussian function $g(t)$ is given by

$$g(t) = \frac{f}{\sqrt{2\pi}} e^{\frac{(\tau-t)^2 f^2}{2}} \ldots\ldots\ldots (3)$$

Combining equations 2 and 3, the S-Transform is defined as

$$S(\tau, f_1) = \int_{-\infty}^{\infty} h(t) \frac{f}{\sqrt{2\pi}} e^{\frac{(\tau-t)^2 f^2}{2}} e^{-i2\pi ft}\, dt \ldots\ldots\ldots (4)$$

As shown in equation 3, $S(\tau, f_1)$ is a one dimensional vector, which contains the changes of amplitude and phase over $h(t)$ for a particular frequencyf_1. This equation is applied to all frequencies within the signal. The net result of the S-Transform is a complex matrix; the rows of that matrix are different frequencies at particular time values (columns).

We also performed a 2D S-Transform analysis by simultaneously running the 1D S-Transform analysis at a specific frequency on all individual locations along the FO-DTS cable and within the imaged volume of the 3D resistivity (to see how the amplitude for a specific frequency within the frequency spectrum changes with time at each location) and also running it at the same time (to see how the amplitude at a specific frequency changes with spatial location). The 2D S-Transform image is produced by averaging the observed results of two successive locations at each time step [*Mansinha et al.*, 1997], and performing this along all locations. This 2D S-Transform depicts the amplitude of the DTS signal at a specific frequency along the DTS cable or within the volume of the resistivity survey.

3D ERT monitoring data processing protocol

ERT monitoring results reported here focus on the 3D survey (#4 in Figure 1) so the processing of these datasets is summarized here.

Data filtering: Each data set was filtered in order to remove noisy measurements. Data were culled if the relative difference between reciprocal measurements exceeded 5% of the observed value, if the injected current was less than 0.01 A, or if the apparent resistivity exceeded 10 kOhm. For time lapse inversion it is also necessary to reduce each time-lapse dataset to a common survey configuration. We used a strict approach for data filtering in this regard whereby if any measurement fell below the quality criteria in any time-lapse data set, that measurement was culled in every data set. Such strict filtering criteria preserves only the data which are consistently high-quality throughout the monitoring period, at the expense of possibly eliminating measurements which are high-quality in most of the time-lapse data sets. We found the data quality decreased with time so that the number of consistent high quality measurements was significantly less than the number of data collected during each time-lapse survey. For instance, during the first 20 days of monitoring 7945 of the 8660 measurements passed the filtering criteria in each data set. After 70 days of monitoring, only 3639 measurements passed the same criteria. We opted to use these 3639 measurements per data set for the time-lapse inversions in order to allow continuous analysis of the entire 70 day monitoring period. We used 273 data sets collected from Nov. 17, 2010 to Feb. 22, 2011 to produce the bulk conductivity time series we compared to river stage in the forthcoming sections.

Inversion processing: Data were weighted according to the criteria proposed by [*LaBrecque and Yang*, 2001] which gives the standard deviation of each measurement as

$$\sigma_i = \alpha\, d_{obs,i} + \beta \tag{5}$$

where σ_i is the standard deviation of measurement i, $d_{obs,i}$ is the observed transfer resistance for measurement i, α is a scalar weighting parameter which scales the standard deviation according to the magnitude of $d_{obs,i}$, and β is a measure of instrument precision and prevents small measurements from having excessively small standard deviations and dominating the inversion. Based on analysis of the reciprocal measurements, we chose $\alpha = 0.05$ and $\beta = 0.001$. We used the normalized χ^2 statistic as the convergence criteria which is given by

$$\chi^2 = \frac{1}{N_d - 1} \sum_{i=1}^{N_d} \left(\frac{d_{pred,i} - d_{obs,i}}{\sigma_i} \right)^2. \tag{6}$$

If the data are appropriately weighted given the actual (but unknown) noise, then $\chi^2 = 1$ when the data are appropriately fit.

To construct the time-lapse sequence we invert the first data set collected Nov. 17, 2010 to produce a baseline conductivity distribution. We regularized this inversion with isotropic first-order spatial derivative smoothing constraints. The results of this inversion serve as both the starting and reference model for the subsequent time lapse inversions. To construct each time-lapse inversion, equation 6 is computed using the predicted data from the starting model and the observed data from the current time lapse data set. If the χ^2 criteria is not satisfied at the starting model, the inversion procedure updates the starting model using a parallel Gauss-Newton

iteration procedure [*Johnson et al.*, 2010]. Each inversion is regularized by both spatial and temporal smoothing constraints. The temporal constraints are provided by minimizing the difference between the baseline and time-lapse solutions. Thus, deviations from the baseline bulk conductivity occur in each time-lapse solution only if required by the data in order to meet the convergence criteria.

We inverted the data using the parallel ERT modeling and inversion code described by [*Johnson et al.*, 2010]. We used an unstructured tetrahedral mesh with refinement near electrodes and within the "imaging zone". The mesh surface topography was constructed using Lidar data collected at the site. The mesh consists of 37,630 nodes and 198,750 elements, and each inversion was executed on 121 processors. The baseline inversion required approximately 30 min of compute time and each time-lapse inversion required between 2 and 10 minutes depending on how far each time-lapse solution deviated from the starting model.

4. Results / Discussion

The results of the project are separated into the four major efforts (1-4) described in Figure 1. We start with the larger scale surveys that focus on the hydrogeologic framework along the river corridor and progressively reduce the investigation scale to finish by examining the focused 3D resistivity study of exchange close to the IFRC.

a. Continuous Waterborne Electrical Imaging (CWEI) for the characterization of the river corridor.

The CWEI proved remarkably successful at determining the spatial variability in the elevation of the H-R contact along the river corridor. In order to illustrate the information content of this spatially rich dataset, Figure 21 shows a cross-section of the river corridor obtained by inverting the CWEI data for Line 20 (located approximately 20 m from the western shore). The normalized chargeability ($M_n = M/\rho$), calculated from the inverted ρ and M model space, is plotted in Figure 21a and the ρ model is shown in Figure 21b. The electrical structure shown in Figure 21 is largely reproduced in the other shore-parallel transects, although image resolution below the riverbed is reduced due to greater water depths further offshore (Figure 21c). We focus on M_n as a lithologic indicator because it is directly proportional to the imaginary conductivity (σ''), an excellent field-scale indicator of lithology [*Slater and Lesmes*, 2002b]. Furthermore, although lithology exerts a strong control on ρ due to variations in ϕ and clay content, ρ also is dependent on σ_w. Given that σ_w varies spatially and temporally in the river corridor as a result of surface-water/groundwater exchange, ρ is generally not considered a robust indicator of lithologic variability. Figure 21 generally shows a 2-layer model composed of a low M_n (high ρ) layer overlying a high M_n (low ρ) layer. The upper layer includes the variable thickness water layer (constrained in the inversion to a layer of constant ρ and zero M). The riverbed is shown as a black line. We attribute the lower, sub-river bottom, part of the upper layer to the Hanford Formation, where the very low M_n is consistent with a coarse-grained aquifer devoid of silt and

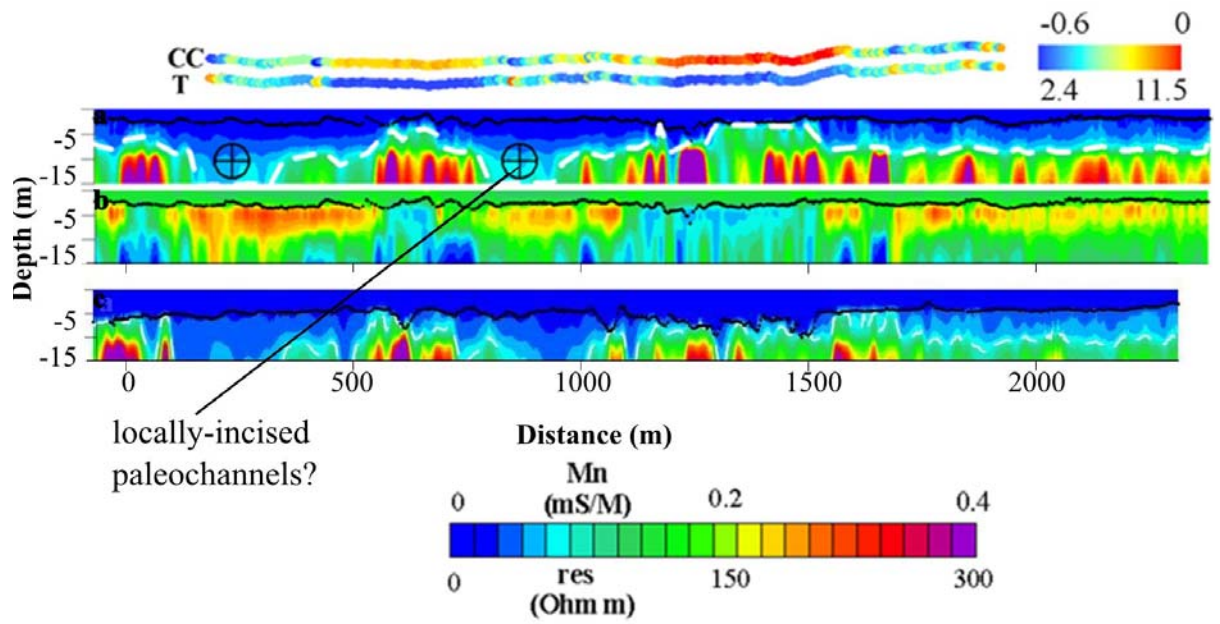

Figure 21. (a) Inverted normalized chargeability (M_n) for continuous waterborne electrical imaging (CWEI) Line 20 (approximately 20 m from shore), (b) inverted resistivity (ρ) for CWEI Line 20. Solid black line denotes the river bed (layer above this is constrained in the inversion) and white dashed line shows the interpreted Hanford–Ringold (H-R) contact. Two locations showing apparently less polarizable deposits eroded beneath the H-R contact (possible paleochannels). Color-coded lines above images for Line 20 show the temperature (T) anomalies and correlation coefficient (CC) for the linear relationship between temperature and stage for data collected March 31, 2009, highlighting that focused exchange is concentrated where the Hanford Formation is thickest. (c) Inverted normalized chargeability (M_n) for continuous waterborne electrical imaging (CWEI) Line 40 (approximately 40 m from shore)

clay. The lower layer is interpreted as the Ringold Formation, where the much higher M_n is consistent with the substantial silt fraction in this unit.

The white dashed line in Figure 21a represents our interpretation of the H-R contact based on the 2-layer electrical structure of the site. As noted previously, the H-R contact is a critical boundary in any hydrogeologic model of the Hanford 300 Area as it limits vertical movement of contaminants in the overlying permeable Hanford unit. CWEI provides an unprecedented characterization of the hydrogeologic setting along this 2.5-km reach of the river corridor at the 300 site, revealing substantial variability in the depth to the H-R contact. In some places, the Ringold appears to be in contact with the riverbed, e.g., between ~1300-1550 m (Figure 21a), which is consistent with estimates of the Ringold exposure on the riverbed based on projection of the H-R contact from inland boreholes combined with point probe tests performed on the riverbed (white outline in Figure 22). However, CWEI captures many details in the lithologic variability along the river corridor not resolvable from the projections based on boreholes and direct probing techniques. For example, the H-R contact is imaged at 5-10 m below the riverbed in some places, and evidence for paleochannels of coarse sediments incised beneath the H-R contact exists at 100-300 m and 750-900 m along this line. Furthermore, the imaging identifies a second location where the Ringold is in contact with the riverbed between 600-700 m that was

not resolved from the borehole projections. Locations where the H-R contact is deepest could represent the presence of local paleo-channels.

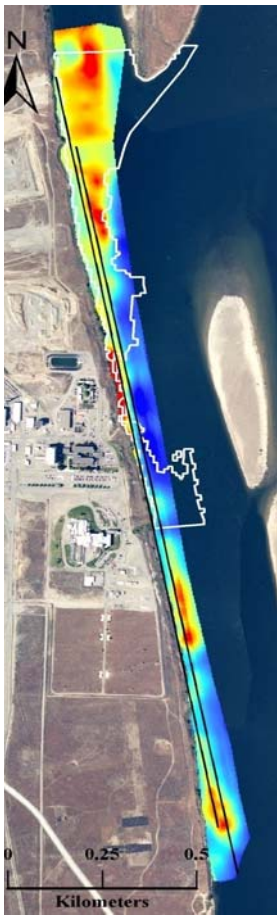

Figure 22. Mn (mS/m) distribution at 7 m depth

Figure 22 shows a plan view spatial distribution of M_n at 7 m depth along the river corridor; the estimated contributing area is superimposed on the map (white outline) [*Fritz et al.*, 2007]. This M_n image was constructed from interpolating the 2D inversion of the CWEI datasets collected along the multiple shore-parallel lines. The inversion slice at 7 m depth was selected as the shallowest (therefore highest resolution) depth that represents the sub-riverbed sediments across the near shore before reaching the channel thalweg where depths rapidly drop to as much as 15 m (Figure 10). The image is cropped east of the edge of the thalweg as it essentially represents only the water layer and contains no useful information. Figure 22 again illustrates the spatial richness of the information that is retrieved from CWEI on the variation in the H-R contact along the river corridor.

Figure 23 compares the distribution of the average streambed temperature during low stage conditions on March 31 (representing winter; Figure 23b) and August 3 (representing summer; Figure 23c) with an estimate of the thickness of the U-contributing Hanford Formation along the river corridor that we derived from the CWEI survey. Whereas the contributing area defined by Fritz et al. (2007) was based on predicted locations where the Hanford Formation is exposed on the riverbed, we utilize the CWEI data to determine variations in the thickness of the Hanford Formation along the river corridor (Figure 23a). This CWEI estimate contains much structure along the corridor that is not captured in the original estimate [*Fritz et al.*, 2007] based on projections of the H-R contact recorded in boreholes.

On the top of Figure 21 we include a snapshot of temperature data (^{o}C) along the river corridor recorded at a time of low river stage during the winter, along with the correlation coefficient (CC) between temperature and the stage of the river recorded for March 31, 2009. The correlation coefficients between temperature and stage for data recorded at 5-min intervals over 8- and 12-day periods in winter and summer respectively, also are shown in Figures 23b and 23c. The DTS dataset highlights focused areas along the river corridor that are anomalously warm during cold months and anomalously cold during warm months. Furthermore, at these locations the temperature is strongly correlated with river stage, with negative correlation in winter (i.e.

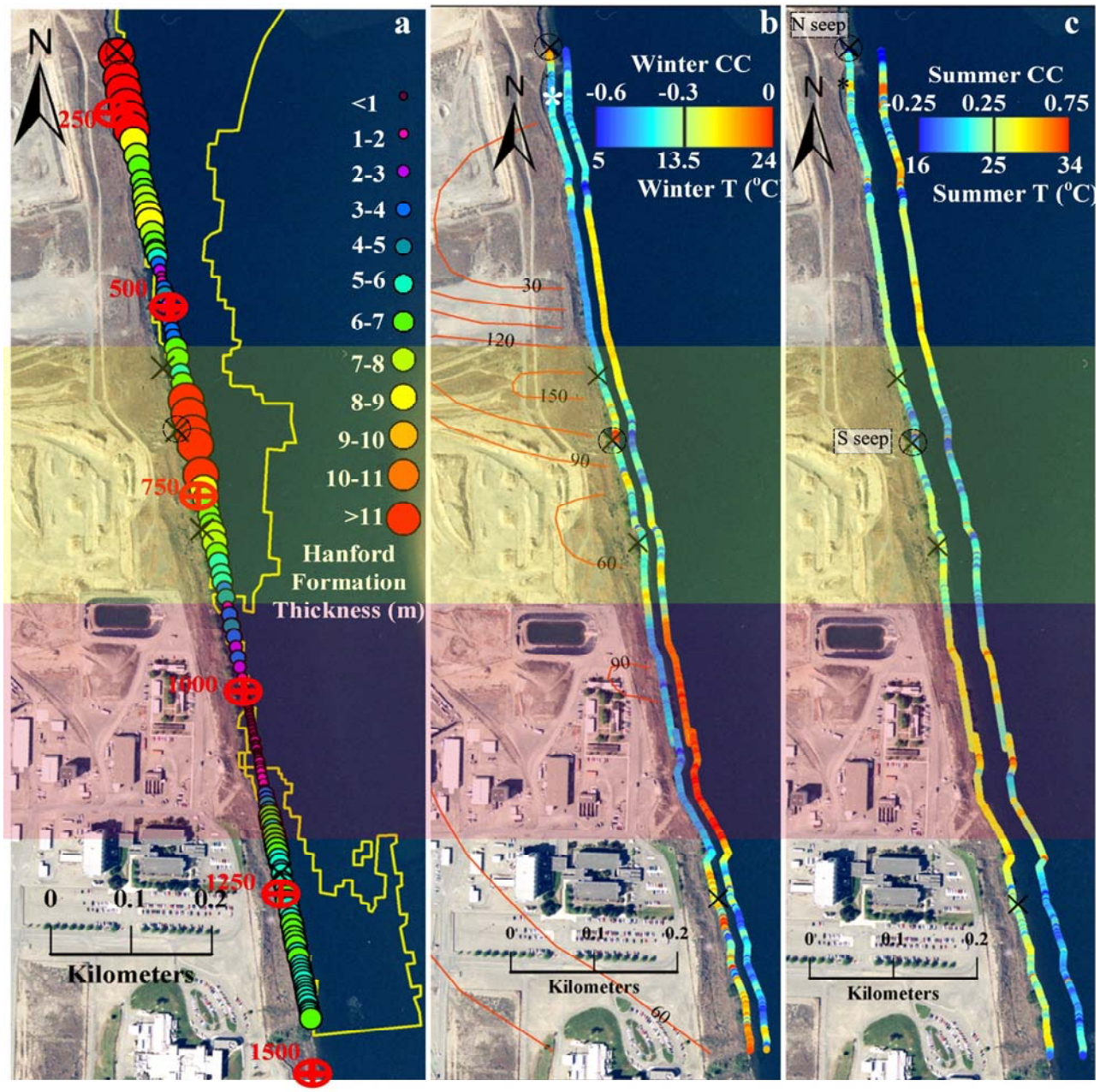

Figure 23. (a) Hanford formation thickness estimated from continuous waterborne electrical imaging measurements. Black crosses show the locations of known springs [*Williams et al., 2007*]. Red crosses indicate distances along the 20m line for comparison with Figure 20; (b) Uranium contours (ug/L) [after *Williams et al., 2007*] and temperature (T) distribution over 1.5 km of fiber-optic distributed temperature sensing (FO-DTS) for measurements at low stage on March 31, 2009; correlation coefficient between temperature and river stage on March 31, 2009 also is plotted (20 m offset for clarity; T is on the left, CC on the right); asterisk shows the area where a structure interpreted as paleochannel was observed with a GPR survey. (c) T distribution over 1.5 km of FO-DTS for measurements at low stage on August 2, 2009; correlation coefficient between temperature and river stage on August 2, 2009 also is plotted (20 m offset for clarity; T is on the left, CC on the right). Yellopw box highlights area of T anomalies, thickest Hanford (estmated with CWEI), known U seeps and high CC whereas the yellow ones is characterized by absence of T anomalies, and U seeps, Ringold exposure to riverbed, and low CC.

higher temperatures as stage falls) and positive correlation (i.e. lower temperatures as stage falls)

in summer. In contrast, away from these anomalies the temperatures on the cable are relatively uniform and uncorrelated with river stage. In summer, weak negative correlation (up to about -0.3) between stage and DTS temperature is evident at some locations, which we interpret as the result of cooler deeper water; thus, the effect of water column temperature acts opposite to that of groundwater discharge, supporting our interpretation that positive correlation in summer is evidence of surface-water/groundwater interaction. The reversal of the anomalies between summer and winter months, along with the strong correlation with river stage at these locations, offers compelling evidence that these are stage-controlled regions of focused surface-water/groundwater exchange. Whereas temperature is a function of many factors (air temperature, solar radiation), we are only interested in the temperature variations arising from hydraulic forcing. Our use of the correlation coefficient between stage and temperature offers a simple analysis of the extensive DTS time series dataset bringing us closer to understanding the processes controlling the discharges identified. Further analysis of the FO-DTS time series is presented later.

The temperature anomalies appear to be correlated with lithology. Considering the CWEI estimate of thickness of the U contributing area (Figure 23a), we see that the temperature anomalies indicating enhanced groundwater exchange coincide with locations along the river corridor where the Hanford sediments are thickest and the Ringold Formation is at depth. These anomalies are closely associated with five known springs/U seeps [*Williams et al.*, 2007], shown as black crosses in Figure 23; circled crosses show the N and S seeps identified in [*Christensen et al., 2010*]. In contrast, temperature anomalies are absent where the Ringold is in contact with or close to the riverbed and no correlation between streambed temperature and stage is observed. The linear correlation coefficient for Hanford thickness as a predictor of temperature-stage correlation is -0.6 and the corresponding Spearman rank correlation coefficient (more appropriate as we have no expectation that the relationship will necessarily be linear) is -0.68. The DTS datasets therefore clearly demonstrate that the lithologic variability imaged with waterborne geophysics is hydrologically important and plays a key role in regulating surface-water/groundwater exchange along the river corridor at the Hanford 300 Area.

This part of our study has illustrated the unique spatially-rich information on surface-water/groundwater exchange at the Hanford 300 Area that comes from integrating CWEI with FO-DTS measurements. These two technologies provide highly complementary information. CWEI images the hydrogeologic framework, primarily the elevation of the H-R contact and the location of possible paleochannel features. In contrast, FO-DTS monitoring identifies areas where surface-water/groundwater exchange is focused. The picture that emerges is distinctly different from that obtained from previous studies based on point observations at boreholes drilled at the 300 Area, along with probing and sampling on the riverbed. [*Fritz et al.*, 2007] noted that their predicted U-contributing area was likely overestimated. Our study shows that there is much spatial variability in elevation of the H-R contact within this estimated contributing area such that exchange likely is enhanced where the Hanford is thickest, and paleochannels

likely are present (Figure 23). Our estimates of regions of focused exchange based on these temperature anomalies coincide with the location of U seeps identified in previous studies. However, the DTS datasets suggest the presence of many additional locations of focused exchange that have not hitherto been recognized from direct sampling.

b. Continuous fiber optic distributed temperature sensing (FO-DTS) monitoring

We have already shown how FO-DTS, coupled with CWEI, is a powerful tool for the spatial characterization of the hydrogeological framework in the 300 area. The high spatial resolution of the FO-DTS, coupled with the high temporal resolution, suggest that this is also an excellent technique for monitoring variations in surface-water groundwater exchange. In this section, we explore the use of the FO-DTS time series further.

Further insight into the dynamics of groundwater-surface water exchange available from the FO-DTS dataset is presented it in Figure 24. The occurrence of the temperature anomalies during low river stage is clear, along with the reversal of these anomalies. During winter high temperature anomalies exist, whereas during summer cold temperature anomalies exist at the same locations. During high river stage the anomalies are absent and the temperature along the profile is uniform and mostly determined by solar heating. The polarity of the anomalies and the

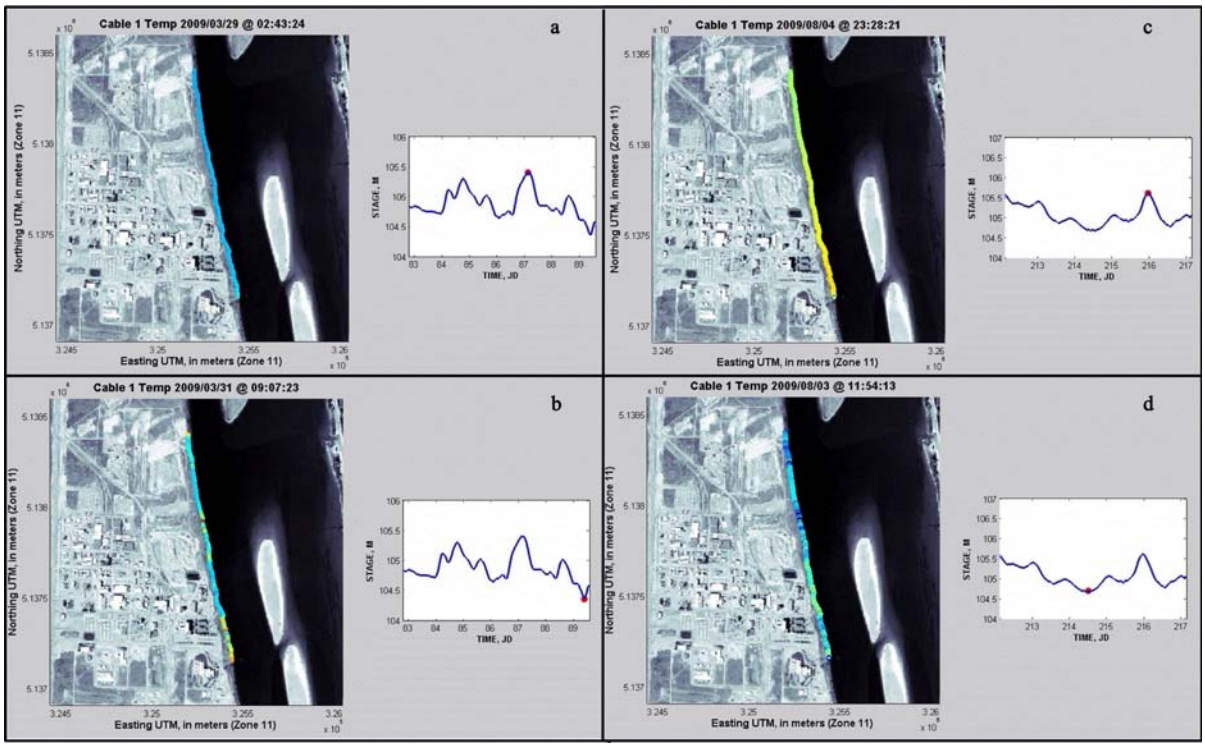

Figure 24. No T anomalies are observed during high stage (a, c); b) warm anomalies, and c) cold anomalies associated with focused groundwater discharge observed during low river stage in cold and warm months respectively.

reversal between summer and winter months provides compelling evidence that they result from focused groundwater discharge along the river corridor. These anomalies are expected to exist only at low stage, when the vertical hydraulic gradient is from the aquifer to the river. During high stage, the vertical hydraulic gradient is presumably from the river into the aquifer and groundwater discharge at the bed is shut off.

Examination of the spatially and temporally variable frequency content of the FO-DTS and stage data using the S-Transform provides further insight into the role of river stage on focused exchange at the river bed. In order to illustrate this, we examine a 24-day time series for two points along the FO-DTS cable as depicted in Figure 25. One of these locations is an identified point of focused exchange where the Hanford Formation is thick. The second location is centered on a region of the cable where exchange is suppressed/non-existent and the Hanford Formation is thin. The time series for these two locations are plotted in Figure 25 for reference. The corresponding stage record for the same time series is also shown as an inset on Figure 25. This highlights the non-stationarity of the river stage variation driven by the dam operations and emphasizes the need for time-frequency analysis e.g. using the S-Transform.

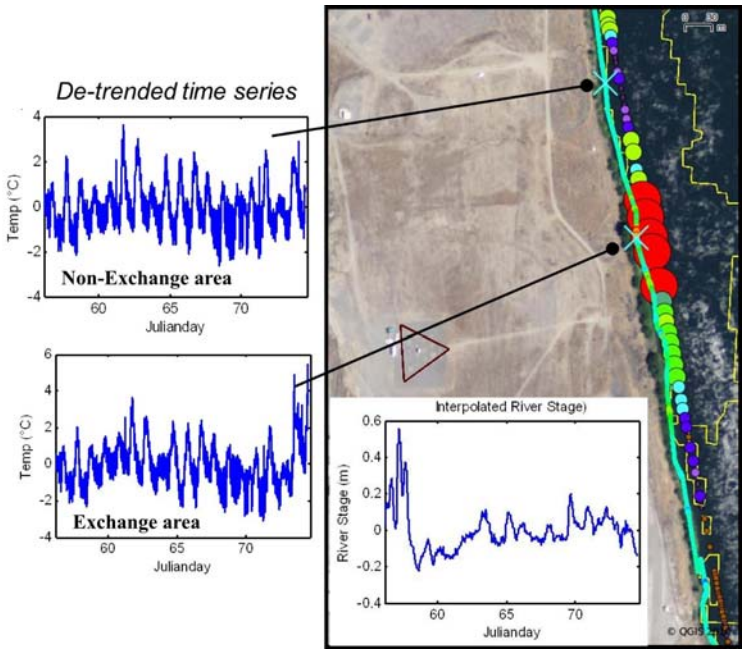

Figure 25. Non–exchange and focused exchange areas chosen for river stage and time series data S Transform analysis.

The S transform analysis for the two locations is shown in Figure 26The S-Transform analysis for the stage dataset is also shown for comparison. The exchange area contains a strong long period (e.g. ~ 4 day) signal that is dominant in the S Transform for the river stage time series. In contrast, these long period signals are very weak at the non-exchange location (Figure 26). The non-exchange location only shows a strong signal for the 1 and 0.5 day periods, reflecting diurnal temperature variations. The S-Transform illustrates how the dominant periodicity of the stage time series is reproduced in the time series at the exchange points, providing solid evidence that stage variations are driving the temperature signals at this location.

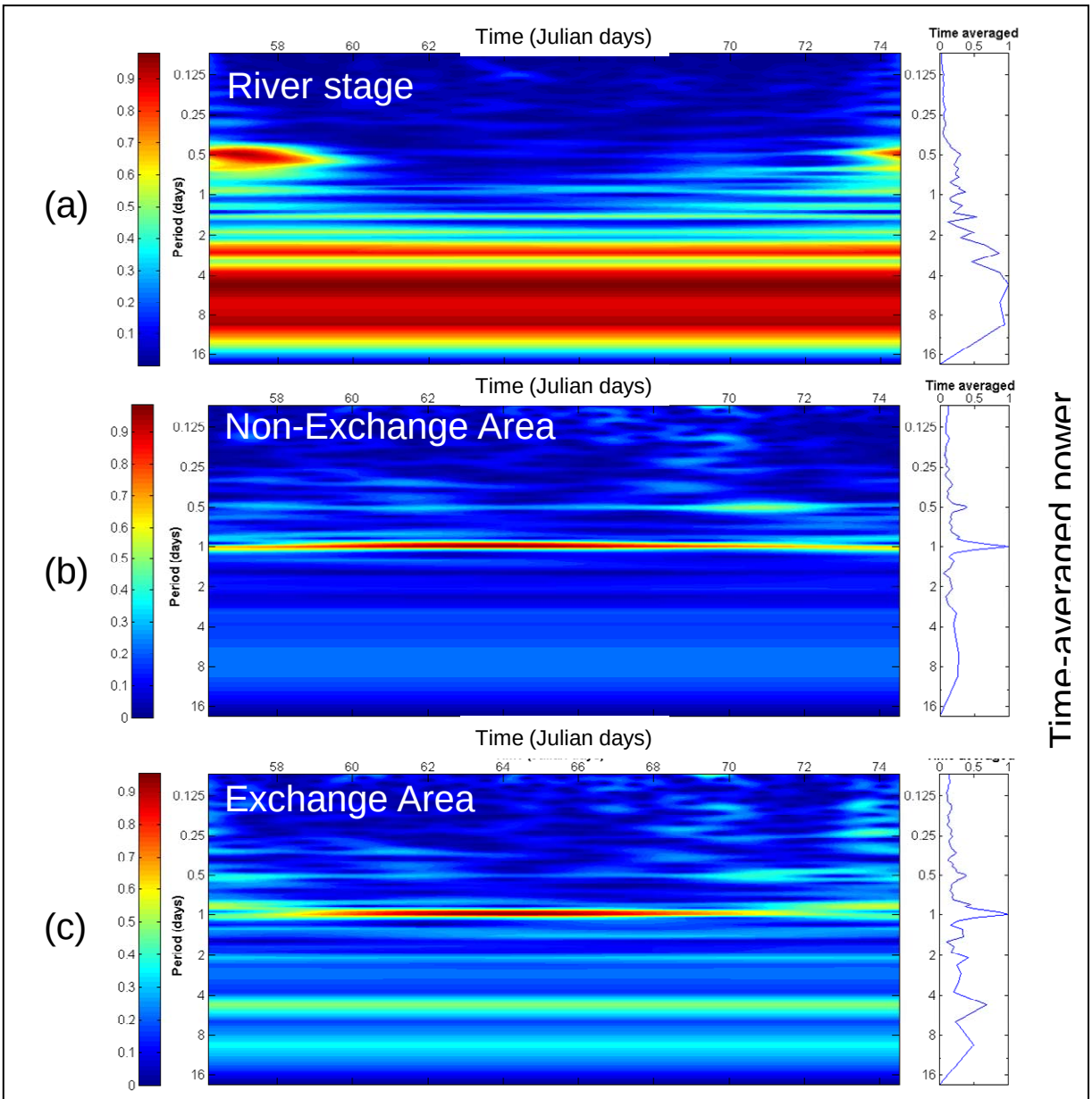

Figure 26. S-Transform analysis of time series shown in Figure 24 (a) stage, (b) temperature at a non-exchange area, (c) temperature at an exchange area.

To extend this analysis further, the S-Transform for all temperature time series making up the

cable (approximately 1.5-2 m interval) is summarized in Figure 27 by showing the spatial variations in the strength of the 4 day and 1 day periods along the cable. Unsurprisingly, the 1 day period is strong and present along the entire period. However, the 4 day period is only present where the Hanford Formation is thickest and is largest at the locations of focused exchange. These images concisely capture the dynamics of the control of river stage on exchange along the river corridor and highlight the role that time-frequency analysis of FO-DTS can play in studies of groundwater-surface water exchange.

c. Land based characterization of the hydrogeological framework local to the 300 Area IFRC.

The land based resistivity and induced polarization (IP) surveys were effective at imaging spatial variation in depth to the Hanford-Ringold contact in the investigated area between the river corridor and the Hanford 300 IFRC. Due to the strong dependence of IP measurements on surface conductivity, we found that IP measurements are an effective method for imaging the lithologic variability across the study area (Figure 28). A detailed evaluation of the application of IP at this site, including the merit of this approach over resistivity imaging and assessment of measurement errors, is presented in [*Mwakanyamale et al.*, In Preparation]. Only key findings of this part of the project are discussed here. Figure 28 shows representative images of the real conductivity (σ'), imaginary conductivity (σ") and phase angle for Line 0, Line 2 and Line 4 with borehole information on the depth to the H-R contact shown where available. The σ' image correlates well with the image of σ", a result that is expected when the complex surface conductivity (σ^*_{surf}), dominates the changes in σ' and σ". However, there is a noticeable contrast

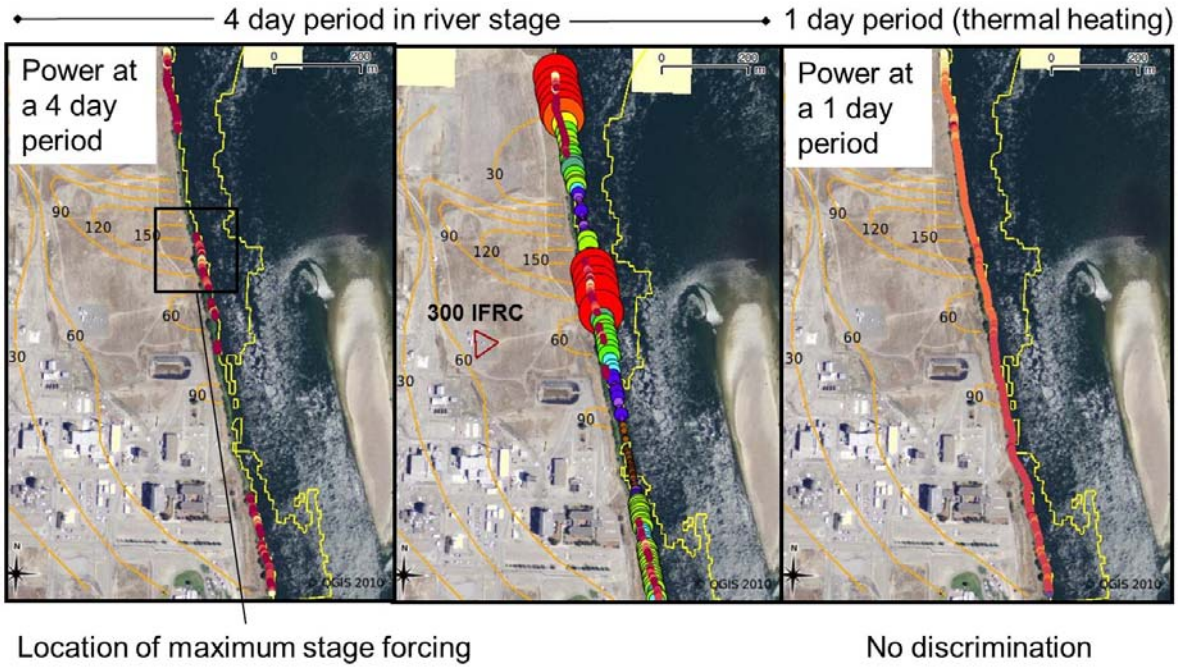

Figure 27. S –Transform analysis at selected frequencies. The 4 day period shows strong correlation between stage changes and focused exchange, while the 1 day period shows no discrimination.

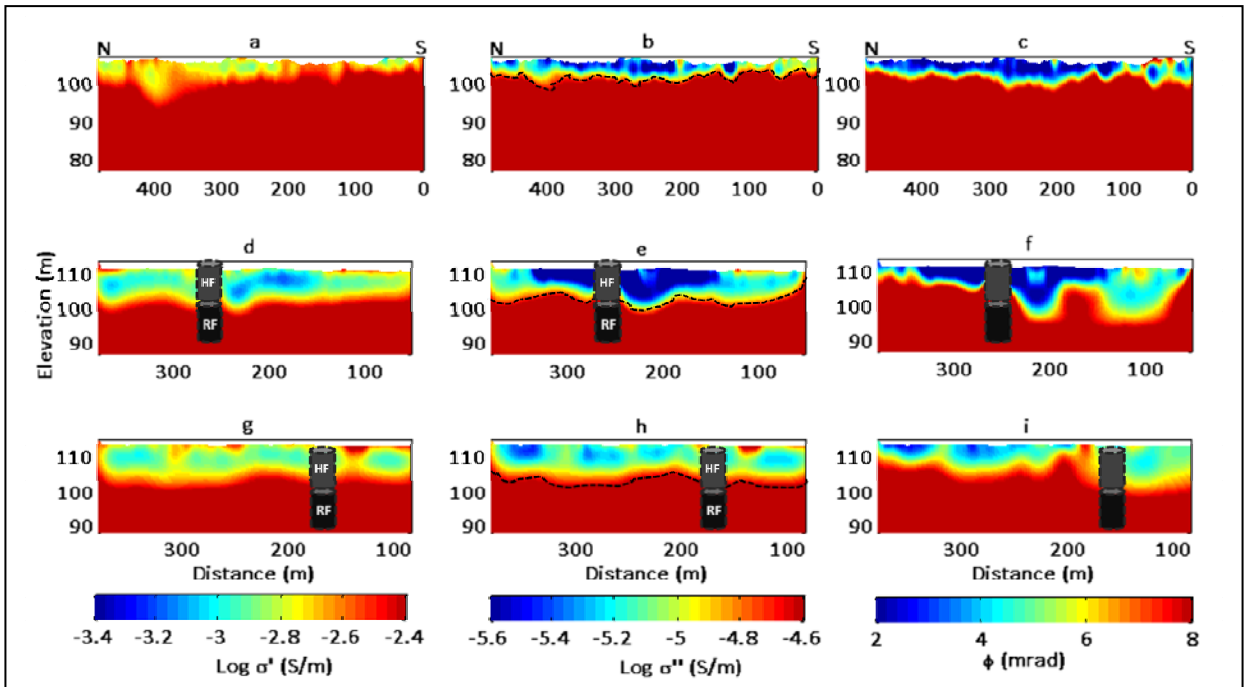

Figure 28. Electrical imaging results from 2D inversion of Line 0 (~10 m from shore), Line 2 (~50 m from shore) and Line 4 (~90 m from shore) showing (a) log σ' of Line 0 (b) log σ" of Line 0(c) ϕ of Line 0(d) log σ' of Line 2(e) log σ" of Line 2 (f) ϕ of Line 2 (g) log σ' of Line 4 (h) log σ" of Line 4 and (i) ϕ of Line 4. Shown on Line 2 and 4 is the location of borehole 399-1-57 and 399-02-01 with H-R contact at 17.6 m and 14.33 m, respectively. Black dashed lines in b, e and h represent the estimated depth to the H-R contact from log σ" at 17.1 m on Line 2 and 12.44 m on Line 4. Note that the log σ' and log σ'' images are both plotted over exactly 1 order of magnitude of variation to illustrate the sharper resolution between the Hanford and Ringold formations in the log σ'' images.

in the sharpness between these two images. The σ" images exhibit a sharper contrast across the contact between the two units than the σ' images. Again, this follows as relative changes in σ" are directly proportional to relative changes in surface conductivity (σ^*_{surf}), whereas relative changes in σ' will be less than relative changes in σ^*_{surf} due to electrolytic conduction. This highlights the benefit of using σ" (and hence IP) for imaging lithology. The sharp contrast in σ" (and σ') across the two units in Figure 28 is expected given the strong contrast in grain size and surface area between the Hanford and Ringold units. The phase ϕ in Figure 28c, 28f and 28i, shows a similar pattern with lowest ϕ in the top (Hanford) layer. Low σ" and small ϕ observed in the upper layer is consistent with low σ^*_{surf} associated with coarse-grained unconsolidated sediments of the Hanford Formation. In contrast, higher σ" and larger ϕ in the bottom layer is consistent with high σ^*_{surf} associated with the fine-grained sediments of the Ringold Formation.

In order to illustrate the information content in this IP survey further, a threshold of log10 σ" (S/m) = -4.7 was applied to the imaginary conductivity images for all lines to represent the transition from the Hanford Formation to the underlying Ringold Formation. This value was selected based on recent laboratory spectral induced polarization measurements on samples acquired from the 300 Area IFRC well field whereby for Ringold cores we consistently

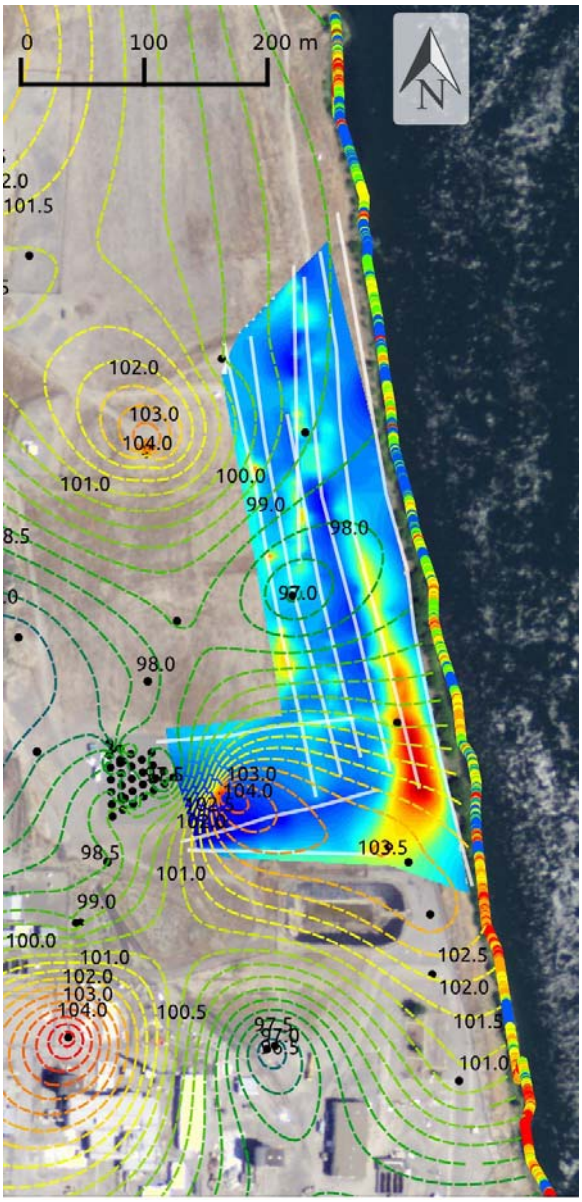

Figure 29. Map view of the HR contact as estimated by resistivity – IP land surveys; superimposed are the H-R contours estimated by borehole data (PNNL 2011); T anomalies based on FO-DTS data are also shown

measured log10 σ" (S/m) > -4.6. The black dashed line in Figure 28 represents the interpreted H-R contact in the σ" images of Line 0, Line 2 and 4 based on this threshold. The position of these lines shows an excellent match to the location of the interface that is visually inferred from the images. Figure 29 is a plan view of the site showing the estimated elevation of the H-R contact between the river and the IFRC area based on this σ" threshold. The overlying contours on Figure 29 represent the elevation of the H-R contact estimated from boreholes scattered across the 300 Area. The estimated H-R elevation from the borehole data ranges from 110.4 m – 89.8 m. Our H-R elevation estimates from σ" threshold offers high resolution estimates compared to the borehole data. The discrepancies between our H-R elevation estimates and the borehole estimates are probably attributed to the small number of boreholes, some of them >100 m apart, that were used to approximate the elevation.

Overall, we estimated the depth to the H-R contact to range from ~19.8 m inland close to the IFRC area to < 5 m in the shallowest parts close to the river. There is evidence of a depression in the H-R contact in the results from 2D inversion. Synthetic modeling described in Mwakanyamale et al. (2011), but not reported here for brevity, demonstrates that the feature is resolvable from the IP dataset given the measured field data errors. A prominent, high resolution depression in the elevation of the contact appears to exist east of the IFRC, turning to run approximately parallel to the river corridor. The size of this depression ~30 m wide, is consistent with expected paleochannel features [*Kunk and Narbutovskih*, 1993] and may represent a paleochannel running parallel with the river from the IFRC area. As proposed earlier, the presence of paleochannels in this study site may result in preferential groundwater-surface water exchange between the 300 Area and the Columbia River. Our results supports this conceptual model due to the fact that the

location where the proposed paleochannel connects with the river corresponds to the enhanced groundwater discharge zones predicted from distributed temperature sensing (DTS) datasets from the 300 Area river corridor (Figure 29).

Results of this work also reveal evidence for heterogeneity in σ^*_{surf} within the Hanford Formation in all lines (see for example Line 4 between 120 - 145 m, 170 –190, 250 and 310 m) (Figure 28). These heterogeneities appear continuous across most lines (not shown for brevity). Such lithologic heterogeneity in the Hanford Formation might be caused by Ringold rip-up clasts that have been observed in sediments retrieved from IFRC boreholes at various depths between 6 – 10 m ([*Bjornstad et al.*, 2009]; http://prc.rl.gov/widl/). As noted by *Bjornstad et al., 2009*, the rip-up clasts contains semi-consolidated, fine-grained sediments similar to the Ringold Formation sediments but cemented with calcium-carbonate. The fine grained, higher surface area rip-up clasts will presumably result in localized higher σ^*_{surf} within the Hanford Formation.

In summary, the land based characterization efforts were very successful in imaging the spatial variations in the elevation of the H-R contact elevation and identifying a prominent depression in the contact that may enhance hydraulic connectivity between the IFRC and the Columbia river. Such data can assist in improving the representation of the hydrologic framework within flow and transport models developed for this site [*Hammond and Lichtner*, 2010].

d. Continuous resistivity monitoring at a hotspot of focused exchange local to the 300 Area IFRC

The results of this part of the work are reported in detail in [*Johnson et al.*, In Preparation] and only summary details are therefore presented here. Results of the baseline inversion are shown in Figure 30. The imaged volume is sliced parallel to the electrode lines and shown with a transparent color scale and an iso-

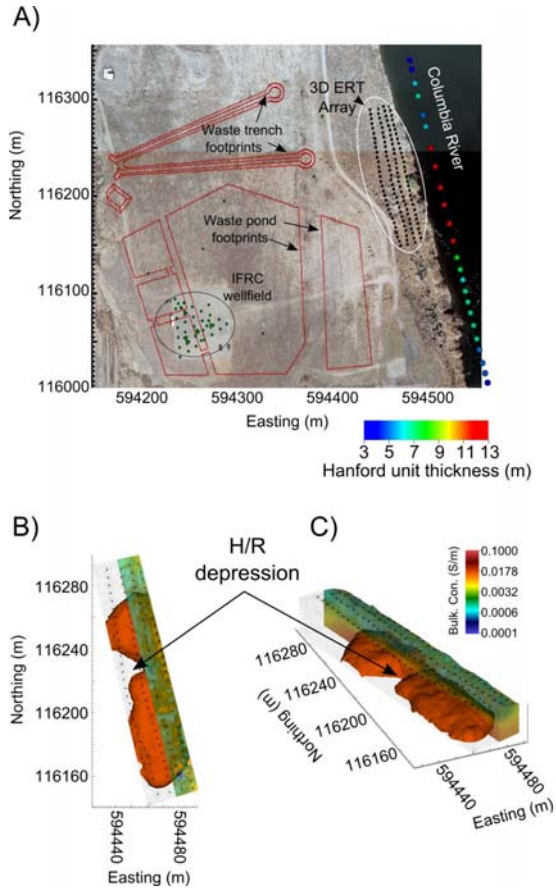

Figure 30. A) Hanford 300 Area, locations of former waste ponds and trenches, IFRC wellfield, Hanford unit thickness [*Slater et al., 2010*], and surface resistivity monitoring array used in this study. B,C) Plan and oblique view of 3D ERT baseline inversion results. The 3D block is sliced to reveal the location of the targeted Hanford/Ringold contact depression (a presumed paleochannel). The bulk conductivity isosurface is at 0.02 S/m

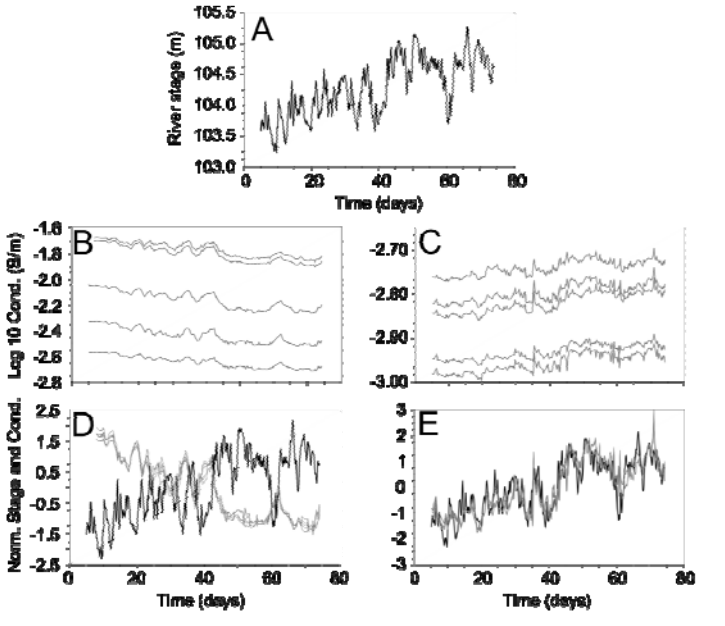

B and D voxel locations (saturated zone)

East. (m)	North. (m)	Elev.(m)
594464.2	116203.8	98.9
594467.1	116227.3	97.6
594468.0	116211.8	93.0
594468.1	116218.3	96.4
594465.7	116210.2	98.8

C and E voxel locations (vadose zone)

East. (m)	North. (m)	Elev.(m)
594462.2	116258.3	106.4
594457.4	116207.4	108.0
594455.3	116249.6	110.1
594450.0	116196.9	111.8
594455.6	116293.4	107.2

Figure 31. A) River stage above sea level with time. B) Example bulk conductivity time series from voxels below the water table with maximum correlation to river stage below -0.85. C) Example bulk conductivity time series from voxels above the water table with maximum correlation values above 0.85. D) Comparison of scaled stage (black) and bulk conductivity for time series (gray) shown in B). E) Comparison of scaled stage and bulk conductivity (black) for the time series (gray) shown in E). The locations of the five voxels below and above the water table are shown below D) and E) respectively.

surface at 0.02 S/m to highlight an indicated depression in bulk conductivity. The depression in the bulk conductivity revealed by the baseline inversion suggests a corresponding depression in the H/R contact, and provides a candidate location for an incised high-permeability paleochannel providing a preferred flow pathway for stage-driven river water intrusion and retreat into and out of the 300 Area. This depression corresponds with a thickening of Hanford sediments in the same location in the river bed identified in the waterborne surveys used to guide placement of the 3D monitoring array and also evident in the larger scale induced polarization imaging survey (figures 18, 20, 22, 23).

Figure 31 shows the river stage over the monitoring period along with the time-series for the bulk conductivity in several voxels that are highly correlated to stage. Figures 31b and 31d show the bulk conductivity time series of examples voxels below the water table, while 31c and 31e show example voxels above the water table. The time series shown in 31d and 31e are scaled by subtracting the mean from each time series and dividing the results by the standard deviation as shown by the correlation computation in equation 1. Example voxel locations corresponding to figures 30b,d and 30c,e are shown below figures 30d and 30e respectively.

Figure 30d demonstrates the typical behavior for voxels in locations that are in hydrologic communication with the river. Bulk conductivity fluctuations show high negative correlation to river stage as expected for groundwater-surface water exchange when the river water is less conductive than the ground water. In addition, we observed a lag time in the bulk conductivity increase/decrease caused by a corresponding decrease/increase in stage. This lag time

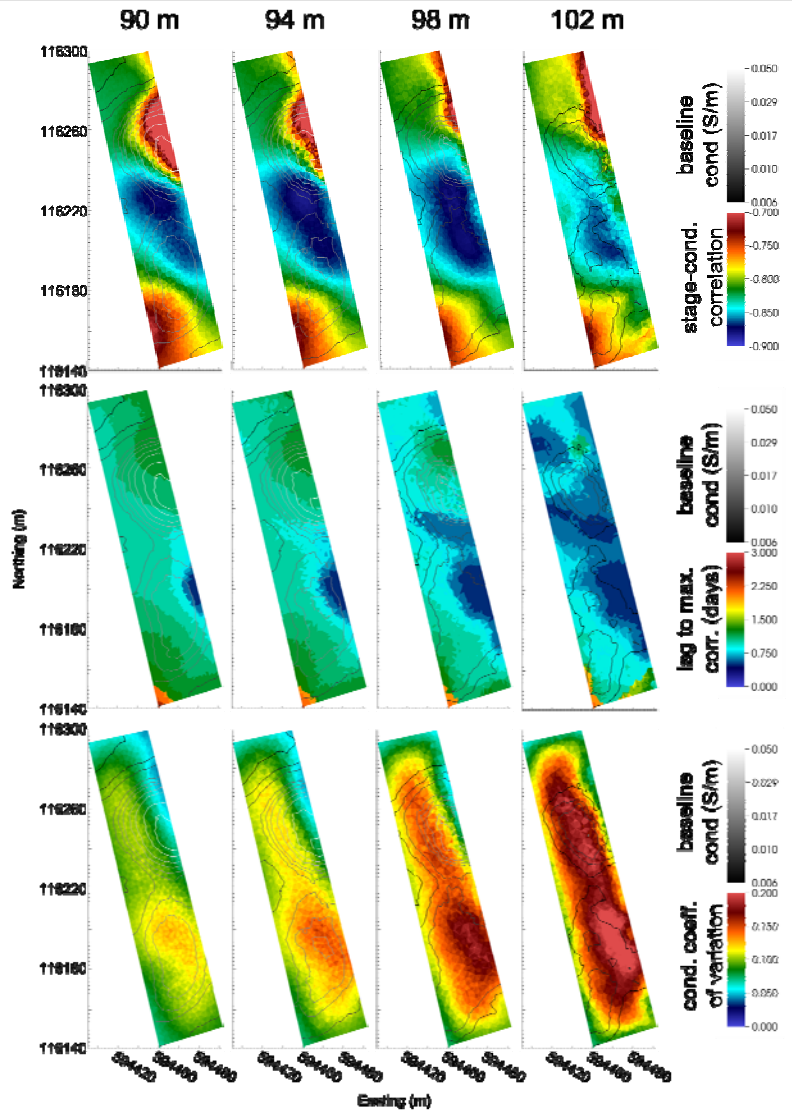

Figure 32. Correlation (top row), lag time (middle row), and coefficient of variation (bottom row) at selected depths below the water table. The grayscale contours show the baseline bulk conductivity superimposed on each plot at depth. Maximum correlations and minimum time lags occur within the presumed paleochannel marked by the baseline bulk conductivity depression.

presumably corresponds to the time required for river water to infiltrate or evacuate the aquifer at the voxel location after an increase or decrease in stage.

Figure 32 shows the maximum correlation, time lag, and coefficient of variation at selected depths beneath the water table. Baseline bulk conductivity contours are superimposed on the images at each depth in order to show the location of the bulk conductivity depression. Bulk conductivity displays a strong negative correlation to stage throughout the saturated zone, ranging from -0.7 to -0.9. This is expected since, for example, river water will eventually replace groundwater throughout the imaging zone during a sustained high stage. Furthermore, the most negative correlations occur directly over the target bulk conductivity depression. Lag time to maximum correlation is arguably the most useful statistic in Figure 32 because it is related to pore water velocity, and therefore to permeability. Lag times are shortest within the bulk conductivity depression at each depth, and shortest overall near the water table (e.g. well above the Ringold formation).

Figure 33 shows the results of applying the S-Transform analysis to (a) the stage time series, (b) a voxel within the vicinity of the depression in the H-R contact where the conductivity-stage correlation is strong, and (c) a voxel well away from the depression in the H-R contact where the conductivity stage correlation is absent. Similar to the observations for the time-frequency

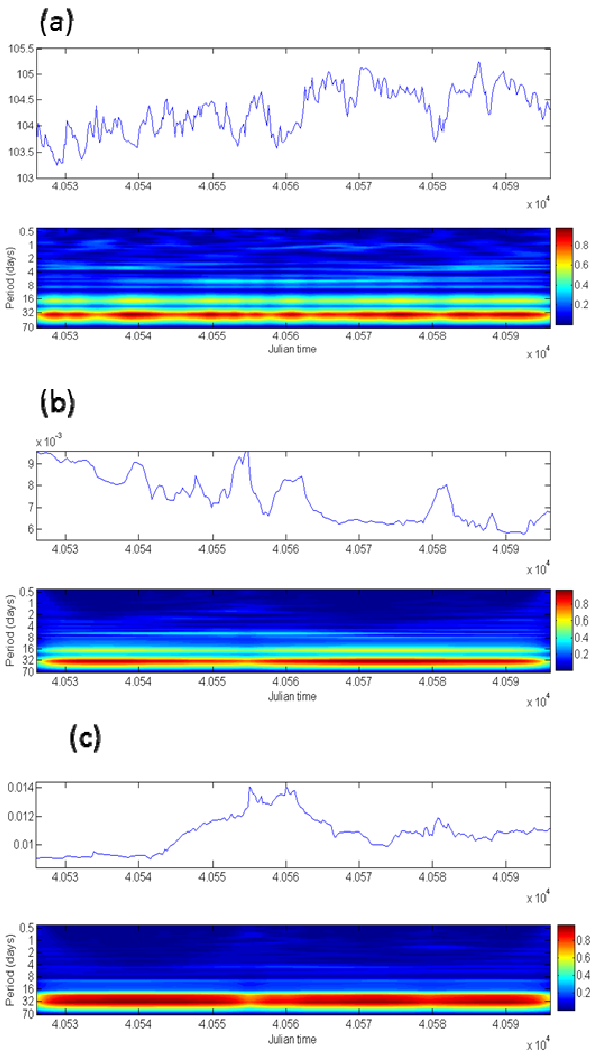

Figure 33: Example time-frequency analysis of the 3D resistivity survey showing S-Transform results of (a) river stage, (b) a voxel within the vicinity of the depression in the H-R contact where the conductivity-stage correlation is strong, and (c) a voxel well away from the depression in the H-R contact where the conductivity stage correlation is absent

analysis of the DTS dataset, the voxel located within the vicinity of the depression contains strong long-period signals that are also present in the stage time series. These periods are approximately 4, 8 and 16 days. In contrast, these periods are absent in the time series for the voxel that is away from the depression. Using a similar approach to Figure 27, the strength of the 8 day period obtained from the S-Transform analysis was determined for every voxel making up the model space. Figure 34shows the result of this analysis at an elevation of 99 m, i.e. above the H-R contact. The boxed region shows the depression in the H-R contact for reference. The image illustrates that the power of this signal in the stage data is concentrated in the vicinity of the depression and is consistent with stage-driven mixing of groundwater and surface water through this zone. Outside of the depression, the normalized power of the S-Transform at this period is small.

The results of this study demonstrate how time series and time-frequency analysis of continuous resistivity monitoring datasets can be used to improve the hydrological content of the information obtainable from electrical imaging of groundwater-surface water exchange. The work demonstrates a novel approach to interpreting autonomous resistivity imaging datasets that contain information on dynamic hydrological processes. The images presented in this section illuminate the role of the identified depression in the H-R contact close to the IFRC in promoting preferential exchange between surface water and groundwater.

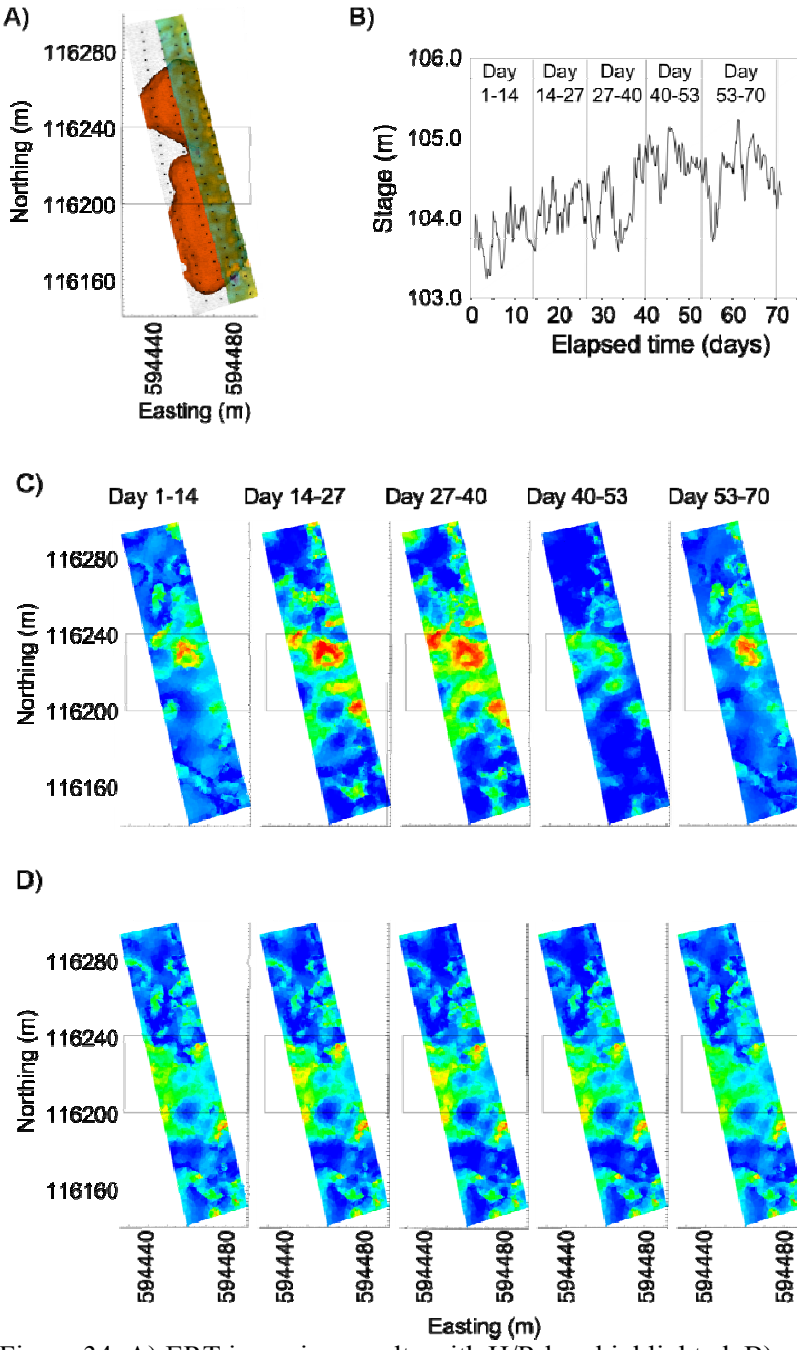

Figure 34. A) ERT inversion results with H/R low highlighted. B) River stage elevation over monitoring period, including time-frequency analysis divisions for comparison to C) and D). C) Normalized power at an elevation of 99 m and a period of 8 days. D) Normalized power at an elevation of 99 m and a period of 16 days. The boxed region shows the H/R low (see part A.)

5. Concluding Remarks

The geophysical characterization and monitoring strategy developed in this project proved successful in yielding new insights into surface water/groundwater interaction at the Hanford 300 Area. The high spatiotemporal resolution of the techniques adopted in this study provided multi-scale information unobtainable with established subsurface investigation methods based on the drilling of boreholes and/or installation of sensors that directly measure groundwater-surface water fluxes. The methods utilized in this study provide indirect information on lithology and groundwater/surface water exchange and should not be considered a ground truth standard. However, the consistency of the information obtained from the different techniques/surveys, combined with the agreement against direct information where available (boreholes, confirmed uranium seeps, etc.) provides confidence in the interpretation of the datasets.

Strategies for extracting the rich hydrological information contained within FO-DTS and 3D resistivity time series based on time series analysis and time-frequency analysis were employed in this work. To the best of our knowledge, this represents the first such interpretation of a 3D time-lapse survey. This approach, which is focused on extracting the signature of the stage variation forcing groundwater/surface water exchange from the geophysical measurements, enhances the hydrological interpretation of the geophysical dataset relative to the traditional examination of a time series of resistivity images. Both FO-DTS and 3D resistivity monitoring could be employed at other DOE sites where groundwater/surface water interaction exerts a control on contaminant flow and transport.

The datasets acquired in this project provide opportunities for future research. Firstly, the potential exists to utilize the spatiotemporally rich information within a coupled hydrological-geophysical inversion framework. The hydrological modeling could be constrained by the soft hydrological information contained within these datasets, in addition to hard information from conventional measurements. Estimates of the H-R thickness obtained from this work provide information that could be used to constrain the representation of the site geology in the PLFOTRAN model that has been developed to model uranium transport from the 300 Area. Efforts to ensure the transfer of information to the modeling community have already begun. For example, P. Lichtner has been provided with estimates of the depth to the H-R contact along 2.6 km of the river corridor obtained from the waterborne imaging. This exchange of information will continue as remaining papers describing the work are completed.

Finally, the results presented strongly encourage further geophysical characterization and monitoring work at the 300 Area. For example, resistivity and IP surveys could be performed on larger grids in order to map the continuity of the depth to the H-R contact from the river corridor and up to the IFRC. Further information on the distribution of depressions in the H-R contact would help to better constrain preferential flow/transport at the site. Resistivity monitoring further inland could address important questions regarding the extent of the zone of groundwater/surface water mixing inland and within the IFRC wellfield. Such work will likely bring important further insight into the dynamics of flow and transport of this important river corridor.

References

Archie, G. E. (1942), The electrical resistivity log as an aid in determining some reservoir characteristiscs, *Transactions of the American Institute of Mining, Metallurgical, and Petroleum Engineers*, *146*, 54-62.

Binley, A., and A. Kemna (2005), Electrical methods, in *Hydrogeophysics*, edited by Y. Rubin and S. Hubbard, pp. 129-156, Speinger, New York.

Bjornstad, B. N., D. C. Lanigan, J. A. Horner, P. D. .Thorne, and V. R. Vermeul (2009), Borehole Completion and Conceptual Hydrogeologic Model for the IFRC Well Field, 300 Area, Hanford Site. Integrated Field Research Challenge Project*Rep. PNNL-18340*, Pacific Northwest National Laboratory, Richland, Washington.

Brown, D. J. (1960), Evaluation of earth samples from churn-drilled wells*Rep. HW--67415*, 12 pp, General Electric Co. Hanford Atomic Products Operation, Richland WA.

Day-Lewis, F. D., K. Singha, and A. M. Binley (2005), Applying petrophysical models to radar travel time and electrical resistivity tomograms: Resolution-dependent limitations, *J. Geophys. Res.*, *110*.

Day-Lewis, F. D., E. A. White, C. D. Johnson, and J. W. L. Jr. (2006), Continuous resistivity profiling to delineate submarine groundwater discharge—examples and limitations, *The Leading Edge*, 724-728.

de Groot-Hedlin, C., and S. Constable (1990), Occam's inversion to generate smooth, two-dimensional models from magnetotelluric data, *Geophysics*, *55*(12), 1613-1624.

de Voogd, N. (1983), Thin-layer response and spectral bandwidth, *Geophysics*, *48*(1), 12.

Denker, H., and H. G. Wenzel (1987), Local geoid determination and comparison with GPS results, *Bulletin Géodésique*, *61*(4), 349-366.

EPA (1996), Declaration of the Record of Decision for the 300-FF-1 and 300-FF-5 Operable Units*Rep.*, Washington, D.C.

Fritz, B. G., N. P. Kohn, T. J. Gilmore, D. McFarland, E. V. Arntzen, R. D. Mackley, G. W. Patton, D. P. Mendoza, and A. L. Bunn (2007), Investigation of the Hyporheic Zone at the 300 Area, Hanford Site*Rep. PNNL-16805*, Pacific Northwest National Laboratory, Richland, WA.

Gamage, N., and W. Blumen (1993), Comparative-Analysis of Low-Level Cold Fronts - Wavelet, Fourier, and Empirical Orthogonal Function Decompositions, *Mon Weather Rev*, *121*(10), 2867-2878.

Grinsted, A., J. C. Moore, and S. Jevrejeva (2004), Application of the cross wavelet transform and wavelet coherence to geophysical time series, *Nonlinear Proc Geoph*, *11*(5-6), 561-566.

Hammond, G. E., and P. C. Lichtner (2010), Field-scale model for the natural attenuation of uranium at the Hanford 300 Area using high-performance computing, *Water Resour Res*, *46*(9).

Hartman, M. J., L. F. Morasch, and W. D. Webber (2006), Hanford Site Groundwater Monitoring for Fiscal Year 2005*Rep. PNNL-15070*, Pacific Northwest National Laboratory, Richland, WA.

Haus, B. K., and H. C. Graber (2000), Analysis of non-stationary vector fields using wavelet transforms, paper presented at Oceans 2000 MTS/IEEE, Holland Publications.

Henderson, R. D., F. D. Day-Lewis, and C. F. Harvey (2009), Investigation of aquifer-estuary interaction using wavelet analysis of fiber-optic temperature data, *Geophys. Res. Lett.*, *36*.

Johnson, T., L. Slater, D.-L. F., and M. Elwaseif. (In Preparation), Monitoring groundwater-surface water interaction using time-series analysis of resistivity datasets, *Water Resour Res*.

Johnson, T., R. J. Versteeg, A. Ward, F. D. Day-Lewis, and A. Revil (2010), Improved hydrogeophysical characterization and monitoring through parallel modeling and inversion of time-domain resistivity and induced-polarization data, *Geophysics*, *75*(4), WA27.

Kunk, J. R., and S. M. Narbutovskih (1993), Phase I Summary of Surface Geophysical Studies in the 300-FF-5 Operable Unit*Rep. WHC-SD-EN-TI-069*, Richland, WA.

LaBrecque, D. J., and X. Yang (2001), Difference Inversion of ERT Data: a Fast Inversion Method for 3-D In Situ Monitoring, *Journal of Environmental and Engineering Geophysics*, *6*(2), 83.

Lesmes, D. P., and K. M. Frye (2001), Influence of pore fluid chemistry on the complex conductivity and induced polarization responses of Berea sandstone, *J Geophys Res-Sol Ea*, *106*(B3), 4079-4090.

Liu, Y. G., X. S. Liang, and R. H. Weisberg (2007), Rectification of the bias in the wavelet power spectrum, *J Atmos Ocean Tech*, *24*(12), 2093-2102.

Loke, M. H., R. I. Acworth, and T. Dahlin (2003), A comparison of smooth and blocky inversion methods in 2D electrical imaging surveys, *Exploration Geophysics*, *34*, 182-187.

Mansinha, L., R. G. Stockwell, and R. P. Lowe (1997), Pattern analysis with two-dimensional spectral localisation: Applications of two-dimensional S transforms, *Physica A*, *239*(1-3), 286-295.

Mansoor, N., and L. Slater (2007), Aquatic electrical resistivity imaging of shallow-water wetlands, *Geophysics*, *72*(5), F211-F221.

Moffett, K. B., S. W. Tyler, T. Torgersen, M. Menon, J. S. Selker, and S. M. Gorelick (2008), Processes Controlling the Thermal Regime of Saltmarsh Channel Beds, *Environmental Science & Technology*, *42*(3), 671-676.

Mwakanyamale, K., L. Slater, A. Binley, and D. Ntarlagiannis (In Preparation), Lithologic Imaging Using Induced Polarization: Lessons Learned from the Hanford 300 Area, *Geophysics*.

Revil, A., and P. J. W. Glover (1998), Nature of surface electrical conductivity in natural sands, sandstones, and clays, *Geophysical Research Letters*, *25*(5), 691-694.

Schon, J. H. (1996), *Physical properties of rocks - Fundamentals and principles of petrophysics*, 600 pp., Pergamon Press, Oxford, OX, UK ; Tarrytown, N.Y., U.S.A.

Selker, J. S., N. Van De Giesen, M. Westhoff, W. Luxemburg, and M. B. Parlange (2006a), Fiber optics opens window on stream dynamics, *Geophys. Res. Lett.*, *33*.

Selker, J. S., L. Thévenaz, H. Huwald, A. Mallet, W. Luxemburg, N. van de Giesen, M. Stejskal, J. Zeman, M. Westhoff, and M. B. Parlange (2006b), Distributed fiber-optic temperature sensing for hydrologic systems, *Water Resour. Res.*, *42*.

Sinha, S., P. Routh, and P. Anno (2009), Instantaneous spectral attributes using scales in continuous-wavelet transform, *Geophysics*, *74*(2), Wa137-Wa142.

Slater, L. (2007), Near Surface Electrical Characterization of Hydraulic Conductivity: From Petrophysical Properties to Aquifer Geometries—A Review, *Surveys in Geophysics*, *28*(2), 169-197.

Slater, L., and D. Lesmes (2002a), Electrical-hydraulic relationships observed for unconsolidated sediments, *Water Resour Res*, *38*(10), 1213.

Slater, L., and D. Lesmes (2002b), IP interpretation in environmental investigations, *Geophysics*, *67*(1), 77-88.

Stockwell, R. G. (1999), S-Transform analysis of gravity wave activity from a small scale network of airglow imagers, University of Western Ontario.

Stockwell, R. G., L. Mansinha, and R. P. Lowe (1996), Localization of the complex spectrum: The S transform, *Ieee T Signal Proces*, *44*(4), 998-1001.

Tsoulis, D. (2003), Terrain modeling in forward gravimetric problems: a case study on local terrain effects, *J Appl Geophys*, *54*(1-2), 145-160.

Tyler, S. W., J. S. Selker, M. B. Hausner, C. E. Hatch, T. Torgersen, C. E. Thodal, and S. G. Schladow (2009), Environmental temperature sensing using Raman spectra DTS fiber-optic methods, *Water Resour. Res.*, *45*.

Waichler, S. R., and S. B. Yabusaki (2005), Flow and Transport in the Hanford 300 Area Vadose Zone-Aquifer-River System*Rep. PNNL-15125*, Pacific Northwest National Laboratory, Richland, WA.

Ward, A. L., and W. P. Clemment (2005), Use of ground penetrating radar to delineate subsurface heterogeneity in the 300-FF-5 Operable Unit*Rep.*, Pacific Northwest Laboratory, Richland, WA.

Weller, A., L. Slater, S. Nordsiek, and D. Ntarlagiannis (2010), On the Estimation of Specific Surface per Unit Pore Volume From Induced Polarization: A Robust Empirical Relation Fits Multiple Datasets, *Geophysics*, *In Press*.

WHC (1993), Sampling and Analysis of 300-FF-5 Operable Unit Springs and Near-Shore Sediments and River Water*Rep.*, Westinghouse Hanford Company, Richland, WA.

White, M. D., and M. Oorstrom (2006), STOMP: Subsurface Transport Over Multiple Phases, Version 4.0.*Rep. PNNL-15782*, Pacific Northwest National Laboratory, Richland, WA.

Williams, B. A., C. F. Brown, W. Um, M. J. Nimmons, R. E. Peterson, B. N. Bjornstad, D. C. Lanigan, R. J. Serne, F. A. Spane, and M. L. Rockhold (2007), Limited Field Investigation Report for Uranium Contamination in the 300 Area, 300 FF-5 Operable Unit, Hanford Site, Washington*Rep. PNNL-16435*, Pacific Northwest National Laboratory, Richland, WA.

APPENDIX 1: LIST OF PRODUCTS AND DELIVERABLES

Journal Articles:

Published

Slater, L. D., D. Ntarlagiannis, F. D. Day-Lewis, K. Mwakanyamale, R. J. Versteeg, A. Ward, C. Strickland, C. D. Johnson, and J. W. Lane, Jr., 2010, Use of electrical imaging and distributed temperature sensing methods to characterize surface water–groundwater exchange regulating uranium transport at the Hanford 300 Area, Washington, **Water Resources Research.**, 46, W10533, doi:10.1029/2010WR009110[1]

In Preparation

Mwakanyamale, K., Slater, L., Binley, A. and D. Ntarlagiannis, Lithologic Imaging Using Induced Polarization: Lessons Learned from the Hanford 300 Area, **Geophysics**, 95% complete and submission planned for August 11'

Johnson, T., Slater, L., Ntarlagiannis, D., Day-Lewis, F. and M. Elwaseif, Monitoring groundwater-surface water interaction using time-series analysis of resistivity datasets, **Water Resources Research**, 75% complete and submission planned for September11'

Dissertations

Mwakanyamale, K., Geophysical characterization and monitoring of groundwater/surface water exchange at the Hanford 300 Area, Department of Earth & Environmental Sciences, Rutgers-Newark, Anticipated Graduation 05/12

Conference Abstracts:

Slater, L., Day-Lewis, F.D., Ward, A., Lane, J., Versteeg, R., Ntarlagiannis, D., Binley, A., Mwakanyamale, K., Johnson, C., Johnson, T. and Elwaseif, M., 2011, Improved Understanding of Groundwater/Surface-Water Interaction at the Hanford 300 Area Using Spatially and Temporally Rich Datasets, 6th Annual Subsurface Biogeochemical Research (SBR) Contractor-Grantee Workshop, Office of Science, Biological and Environmental Research, U.S. Department of Energy, Mar, 2011, Washington, D.C., Abstract

Mwakanyamale, K, Slater, L., Ntarlagiannis, D., Binley, A., Day-Lewis, F. (2011), Use of Time-Domain Induced Polarization for Lithology Identification: Case Study from the Hanford 300-Area, Proceedings of the Symposium on the Application of Geophysics to Engineering and Environmental Problems, Charleston, SC, April 10-14

[1] THIS ARTICLE WAS SELECTED AS AN AGU RESEARCH HIGHLIGHT AND A WRITE UP APPEARED ON THE BACK COVER OF THE WEEKLY AGU MAGAZINE EOS. IT WAS ALSO A HIGHLIGHTED PAPER IN WATER RESOURCES RESEARCH

L. D. Slater, F. D. Day-Lewis, D. Ntarlagiannis, K. E. Mwakanyamale, T. C. Johnson, M. H. Alwasif, A. L. Ward, R. Versteeg, A. Binley and J. Lane (2010), Examination of groundwater-surface water interaction at the Hanford 300 Area using time-lapse resistivity imaging and distributed temperature sensing, Abstract H34A-03 presented at 2010 Fall Meeting, AGU, San Francisco, Calif., 13-17 Dec

K. E. Mwakanyamale, L. D. Slater, D. Ntarlagiannis, A. Binley, F. D. Day-Lewis, A. L. Ward, J. Heenan and E. Placencia (2010), Use of the Time-Domain Induced Polarization Method to Map the Spatial Distribution and Depth of the Hanford-Ringold Contact in the Hanford 300 Area: Results From 2D Complex Resistivity Inversion, Abstract H23C-1199 presented at 2010 Fall Meeting, AGU, San Francisco, Calif., 13-17 Dec

Slater, L., Ntarlagiannis, D., Day-Lewis, F.D., Mwakanyamale*, K., Lane, J.W., Jr., Ward, A. and Versteeg, R., 2010, Use of induced polarization to characterize the hydrogeologic framework of the zone of surfacewater/groundwater exchange at the Hanford 300 Area, WA, 23rd SAGEEP, Environmental and Engineering Geophysical Society (SAGEEP), April 11-15, Keystone, CO

Slater, L., Day-Lewis, F., Ward, A., Lane, J., Jr., Versteeg, R., Binley, A., Ntarlagiannis, D., Mwakanyamale*, K. and Johnson, C., 2010, Geophysical Characterization and Monitoring of Groundwater/Surface-Water Interaction in the Hyporheic Corridor at the Hanford 300 Area, Subsurface Biogeochemical Research (SBR) Contractor-Grantee Workshop, Office of Science, Biological and Environmental Research, U.S. Department of Energy, Mar 29-31, 2010, Washington, D.C., Abstract

L. D. Slater, F. Day-Lewis, D. Ntarlagiannis, K. E. Mwakanyamale*, R. J. Versteeg, A. L. Ward, C. E. Strickland, C. Johnson, J. W. Lane and A. M. Binley, 2009, “Hydraulic Characterization of the Hyporheic Corridor at the Hanford 300 Area Using Geoelectrical Imaging and Distributed Temperature Sensing (DTS) Methods”, Eos Trans. AGU, 90(52), Fall Meet. Suppl., Abstract H53J-05

Mwakanyamale, K., Slater, L., Ntarlagiannis, D., Ward, A. Day-Lewis, F., Johnson, C. , Strickland, C. , Lane, J. Versteeg, R. 2009, Imaging the Zone of Interaction between Hanford Site Groundwater and the Columbia River Using Geophysical Techniques: Results from the Hanford Site 300 Area, National Association of Black Geologists and Geophysicists (NABGG) Annual meeting, September 9-12, 2009, Fayetteville, Arkansas

Slater, L., Day-Lewis, F., Ward, A., Lane, J., Versteeg, R., Ntarlagiannis, D., Mwakanyamale*, K., Johnson, C. and Strickland, C., 2009, Geophysical characterization and monitoring of groundwater-surface water interaction in the hyporheic corridor at the Hanford 300 Area, DOE-ERSP 4th Annual PI Meeting, April 20-23, 2009, Abstract

Mwakanyamale, K., Slater, L., Ntarlagiannis, D., Ward, A., Day-Lewis, F., Johnson, C., Strickland, C., Lane, J. and Versteeg, R., Geophysical characterization of paleochannels within the hyporheic corridor, Hanford 300 Area, DOE-ERSP 4th Annual PI Meeting, April 20-23, 2009, Abstract

Invited Talks:

"Understanding spatiotemporal variability in groundwater/surface-water exchange at the Hanford 300 Area using time-lapse resistivity and distributed temperature sensing**",** Novel Methods for Subsurface Characterization and Monitoring; From Theory to Practice (NovCare), Brewster, MA, May 9-11, 2011 (KEYNOTE, delivered by Slater)

"Joint application of electrical geophysics and distributed temperature sensing (DTS) to study the groundwater-surface water interface at the U.S. Department of Energy's Hanford Facility, USA", RiskPoint Fall International Workshop: Assessing the Risks Posed by Point Source Contamination to Groundwater and Surface Water Resources, Copenhagen, Denmark, October 5-6, 2009 (KEYNOTE, delivered by Slater)

"Examination of groundwater-surface water interaction at the Hanford 300 Area using time-lapse resistivity imaging and distributed temperature sensing", Fall Meeting, American Geophysical Union (AGU), Dec 15, 2010 (delivered by Slater)

"Hydraulic Characterization of the Hyporheic Corridor at the Hanford 300 Area Using Geoelectrical Imaging and Distributed Temperature Sensing (DTS) Methods", American Geophysical Union Fall Meeting, Dec 18, 2009 (delivered by Slater)

"Waterborne IP imaging of Columbia River sediments: geophysical characterization of the hyporheic corridor at the Hanford site", EEGS-NSGS EEGS NSGS Workshop on Induced Polarization: Research and Recent Advances in Near Surface Applications, Nov. 14, 2008, Las Vegas, NV (delivered by Slater)

"Geophysical Characterization and Monitoring of Hydrologic Properties and Processes: Recent Advances and Case Studies," ISCMEM Interagency Steering Committee on Multimedia Environmental Modeling, October 13, 2009, Public Workshop and Meeting, Nuclear Regulatory Commission, Rockville, MD (delivered by Day-Lewis).

"Distributed Temperature Sensing in Hydrology: Case Studies using an Emerging and Evolving Technology," Dept. of Environmental Science, Lancaster University, July 2, 2009 (delivered by Day-Lewis).

"Geophysical monitoring of natural and engineered hydrologic processes," K. Douglas Nelson Lecture Series, Dept. of Earth Sciences, Syracuse University, November 12, 2009 (delivered by Day-Lewis).

“Using geophysical methods to characterize/monitor the hyporheic corridor at the Hanford Site (300 Area”), School of Earth and Environmental Sciences, Queens College (CUNY), October 5, 2009 (Delivered by Ntarlagiannis)

Other Presentations:

"Fiber-optic distributed temperature sensing in the USGS: Applications and Capabilities," U.S. Geological Survey, Office of Groundwater Cyber Seminar Series, October 7, 2009. (delivered by Day-Lewis)

Mwakanyamale, K., Slater, L., Ntarlagiannis, D., Ward, A. Day-Lewis, F., Johnson, C. , Strickland, C. , Lane, J. Versteeg, R. 2009, Imaging the Zone of Interaction between Hanford Site Groundwater and the Columbia River Using Geophysical Techniques: Results from the Hanford Site 300 Area, National Association of Black Geologists and Geophysicists (NABGG) Annual meeting, September 9-12, 2009, Fayetteville, Arkansas [invited student paper]

Slater, L., Day-Lewis, F., Ward, A., Lane, J., Versteeg, R., Ntarlagiannis, D., Mwakanyamale*, K., Johnson, C. and Strickland, C., 2009, Geophysical characterization and monitoring of groundwater-surface water interaction in the hyporheic corridor at the Hanford 300 Area, DOE-ERSP 4th Annual PI Meeting, April 20-23, 2009, Abstract

Mwakanyamale, K., Slater, L., Ntarlagiannis, D., Ward, A., Day-Lewis, F., Johnson, C., Strickland, C., Lane, J. and Versteeg, R., Geophysical characterization of paleochannels within the hyporheic corridor, Hanford 300 Area, DOE-ERSP 4th Annual PI Meeting, April 20-23, 2009, Abstract

APPENDIX 2: Example Results from Continuous Waterborne Surveys (CWS)

1. Ground Penetrating Radar (GPR)

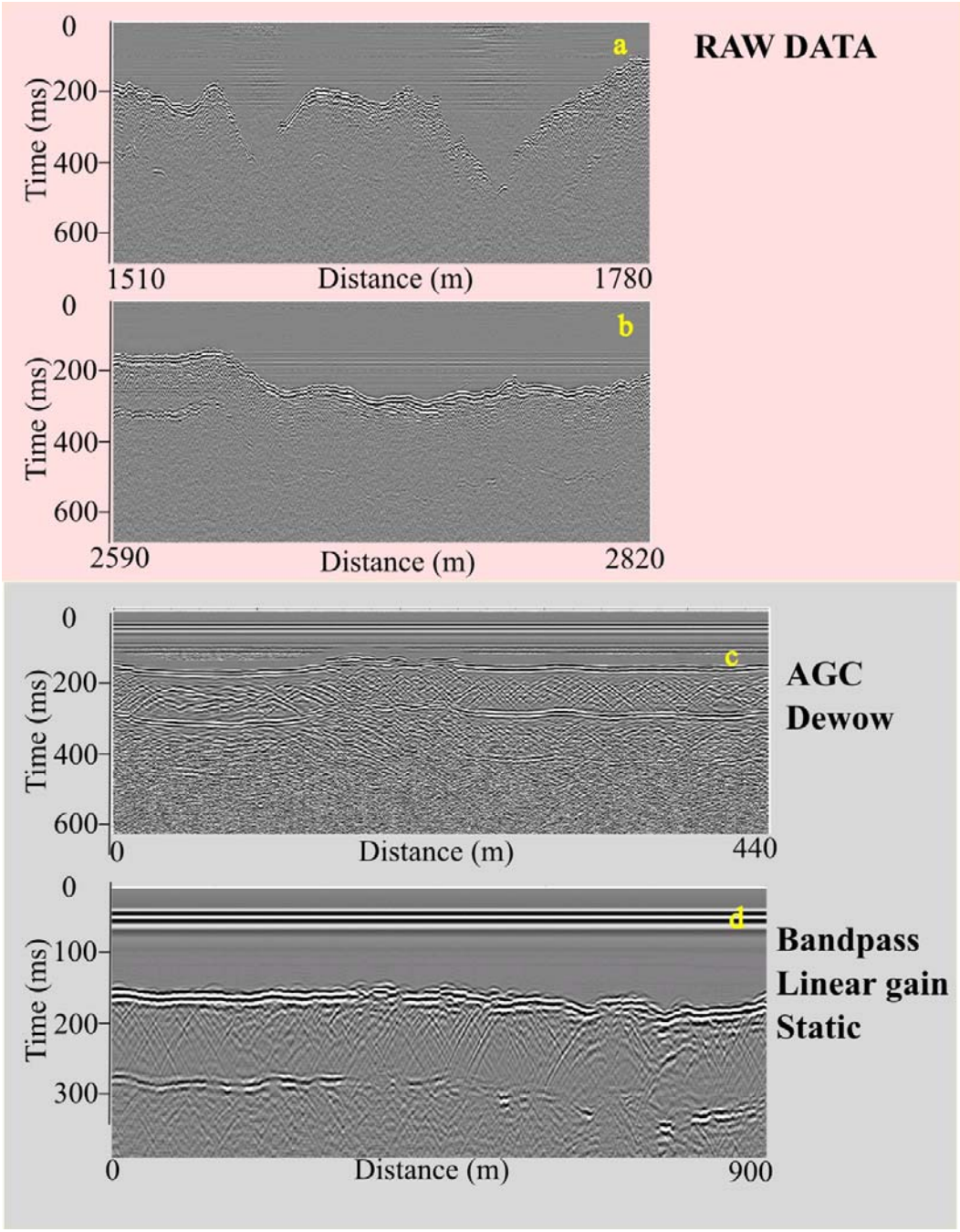

Figure A1. Characteristic data from the CWS GPR surveys. aand b show 2 samples of raw collected data. Data processing improved the visualization of the results but not enough to provide useful information for our project. Two examples are shown where the AGC and dewow (c), and bandpass, static and linear gain (d) filters applied.

2. Seismic

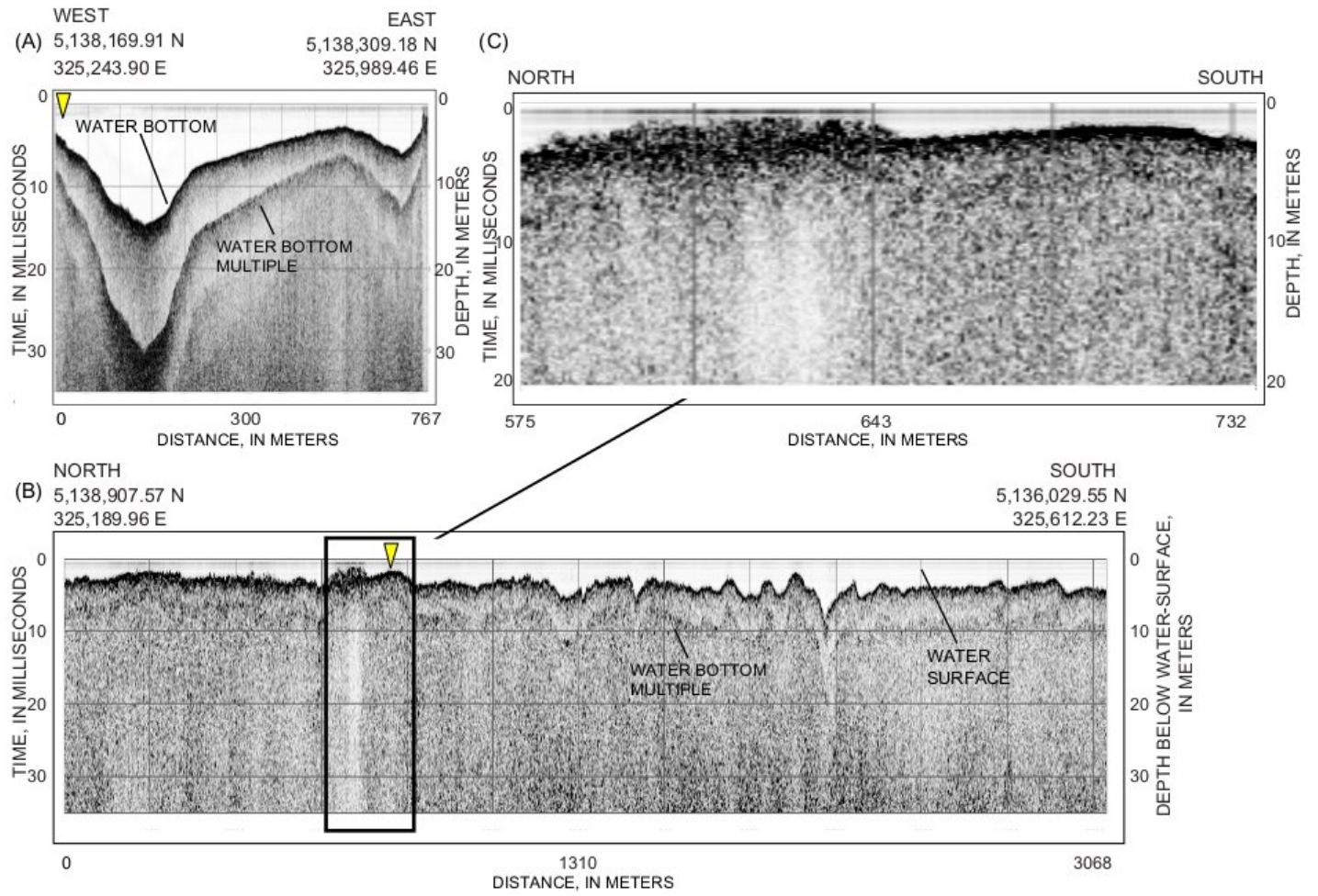

Figure A2. Swept-frequency seismic section, Columbia River at Hanford IFC, Hanford, Washington. (A) Unprocessed data from a profile run west-to-east.(B) Profile run north-to-south. Yellow triangle indicates where sections from (A) and (B) intersect. (C) More detail of a section of the north-south profile. Velocity of sound in freshwater sediments was set to 1,500 meters/second and used to estimate depth. Inverted yellow triangles indicate intersection of water-borne seismic profiles. Depths are shown in meters below transducer, which was 0.6 m below the water surface. End-point positions are in Universal Transverse Mercator using the WGS-84 datum.